

Dynamic Assimilation of MODIS-Retrieved Humidity Profiles within a Regional Model for High-Latitude Forecast Applications

XINGANG FAN

Geophysical Institute, University of Alaska Fairbanks, Fairbanks, Alaska

JEFFREY S. TILLEY

Regional Weather Information Center, University of North Dakota, Grand Forks, North Dakota

(Manuscript received 13 April 2004, in final form 2 May 2005)

ABSTRACT

A “hot start” technique is applied to the fifth-generation Pennsylvania State University–National Center for Atmospheric Research (PSU–NCAR) Mesoscale Model (MM5) to dynamically assimilate cloud properties and humidity profiles retrieved from the Moderate Resolution Imaging Spectroradiometer (MODIS) instrument on board the NASA Earth Observing System polar-orbiting satellites. The assimilation approach has been studied through extensive numerical experimentation for high-latitude rain events to demonstrate the feasibility and the benefit of the approach on the model cloud and precipitation simulation/forecast.

The ingestion of MODIS-retrieved cloud and clear-air humidity information impacts MM5 cloud fields on both a microphysical and macrophysical level. From short-term (6–12 h) forecast experiments conducted for a preliminary test case and 16 extensive summer and winter experiments, the following primary conclusions have been reached. 1) It is feasible to introduce MODIS-retrieved cloud-top properties and humidity profiles into the MM5 model in a hot start mode without disrupting model stability and evolutionary continuity. 2) The introduction of high-resolution MODIS information produced more accurate humidity fields and resulted in increased mesoscale structure in the cloud and precipitation fields. 3) The opportunistic ingestion of MODIS data at its observation time into the model leads to improved 6–12-h model precipitation forecasts with respect to not only the frequency of occurrences, but also the magnitude of precipitation amounts. 4) Verification with three-dimensional analyses indicates some improvement in model forecasts of temperature, wind, pressure perturbation, and sea level pressure as well. 5) Verification with surface station observations indicates that model forecasts of 2-m temperature, 2-m relative humidity, 10-m winds, and sea level pressure are also improved, most notably for the summer cases. The largest improvement in forecast skill is for 2-m relative humidity (12%).

1. Introduction

A continuing problem with respect to regional weather and climate model simulations relates to the fact that simulated cloud fields are often inaccurate. Small perturbations in the amount (fraction, liquid or ice water path, or optical depth) or radiative properties of clouds may induce deviations in the evolution of the simulated atmosphere. The subsequent effects on radiation and energy flow can then in turn strongly affect the model climate (Randall et al. 1984; Slingo 1990). As

noted by Lipton (1993), Lipton and Modica (1999), Ruggiero et al. (2000), and many others, surface energy exchanges, which depend on overlying clouds, have a strong impact on the mesoscale processes that most strongly affect the short-term prediction of clouds and precipitation.

With the exception of the recent study of Bayler et al. (2000) and those data assimilation systems that are set up in a cycling mode, few mesoscale modeling systems are constructed to provide for a proper initialization of cloud hydrometeor fields (e.g., cloud water, ice and snow mixing ratios, and rainwater). Thus, the model must spin up these variables, and their associated cloud systems and latent heating, from other initial fields during the first few (0–6) hours of simulation. This type of

Corresponding author address: Xingang Fan, Geophysical Institute, University of Alaska Fairbanks, 903 Koyukuk Dr., P.O. Box 757320, Fairbanks, AK 99775-7320.
E-mail: xfan@gi.alaska.edu

model start-up is referred as a “warm start” in this paper. Adjustments to the other fields that result from this spinup process of a “warm started” model may result in an erroneous simulation or lead to a degraded forecast in the first few hours. As an example of the fifth-generation Pennsylvania State University–National Center for Atmospheric Research (PSU–NCAR) Mesoscale Model (MM5; Grell et al. 1994; Chen and Dudhia 2001) and the case that are described in the next section, Fig. 1 shows model total precipitable water, column-integrated cloud water and ice, column-integrated rainwater and snow, and accumulated rainfall within two boxes (shown in Fig. 4b) from three model runs: one is started from 1800 UTC 13 August 2001 (ContC-6), one starts 6 h later (CtrlC0), and the third one starts from the same time as CtrlC0 but with MODIS information assimilated (hotMODC0), which will be discussed later. ContC-6 continuously runs through the initial time of CtrlC0. (Refer to Fig. 4b satellite observed cloud coverage, box 1 and box 2 located in clear and cloudy areas, respectively.) It is indicated that even though the CtrlC0 produces the cloud and precipitation mass and adjusts closer to the continuous run ContC-6, the differences between the two model runs are still significantly large. Although the model forecast error of the ContC-6 run is contributing to the above stated differences, the error from the initializing of the warm start of the CtrlC0 run is not negligible. This is one reason that motivates the “hot start” study. Moreover, due to the complex nonlinearity of atmospheric models, initial errors affect model evolutions (Lorenz 1963). Therefore, the best possible forecasts, all other things being equal, should result from minimizing the length of this spinup period. If the model initial state were to contain clouds (via associated hydrometeor mixing ratio fields) that are distributed realistically in three-dimensional space, the model initial state would be much closer to that of the real atmosphere and allow for minimal spinup time, which in theory should lead to improved simulations within the first few hours as well as for later periods.

As an example, we consider the MM5 model, which is widely used for research and real-time forecast applications (e.g., Mass et al. 2003; Powers et al. 2003). The MM5 model contains convective parameterizations (e.g., Grell 1993) to represent subgrid-scale redistribution of heat, moisture, and momentum as well as bulk microphysical schemes to explicitly reproduce stratiform cloud processes (e.g., Reisner et al. 1998). However, the standard version of MM5 is constrained by a need to spin up cloud systems, an important limitation for short-range real-time forecast applications. To address this concern, Fan and Tilley (2003) applied an

explicit moisture scheme (Reisner et al. 1998) to do a static cloud initialization for the MM5 model. Their study further demonstrated how the cloud initialization (or lack thereof) can affect the model initial states of cloud hydrometeors and that the amount of spinup time could be somewhat reduced. The precipitation forecasts of the first 3 h were improved by utilizing the cloud initialization; however, the magnitude of improvement was limited by the coarse resolution of the initial condition fields ($2.5^\circ \times 2.5^\circ$ latitude and longitude) relative to the model grid resolution (45- and/or 15-km grids).

The accuracy of such a static cloud initialization relies heavily on the accuracy of the initial moisture field, since an accurate prediction/depiction of the ambient moisture distribution is a necessary, though not always sufficient, condition for obtaining accurate clouds. Remotely sensed data from satellites can be utilized in areas where conventional observations are sparse, such as the polar regions and midlatitude oceans. It is now recognized that incorporating satellite data into the numerical weather forecast models can yield improved depiction of mesoscale cloud radiative properties and precipitating systems (e.g., Yucel et al. 2003; Key et al. 2003; Fan and Tilley 2002). Satellite data have been assimilated in these studies to supplement surface observations and to improve the model initial conditions or to constrain numerical model evolution.

Fan and Tilley (2002) assimilated the (Advanced Very High Resolution Radiation) AVHRR-retrieved cloud-top brightness temperatures for infrared channel 4 ($11 \mu\text{m}$) into an MM5 analysis to adjust the model moisture fields. [A detailed description of the technique that is adapted and improved for the Moderate Resolution Imaging Spectroradiometer (MODIS) data assimilation is given in section 3.] Their results, obtained for a high-latitude heavy rain case, showed that satellite observations often provide adequate information to benefit cloud forecasts. Continuous, near-continuous, or intermittent (e.g., Fan and Tilley 2002) assimilation of satellite data improved the simulation for a longer time range (~ 24 h). Yucel et al. (2002, 2003) assimilated the Geostationary Operational Environmental Satellite (GOES) cloud-cover fraction into mesoscale models. However, all of these studies utilized a one-layer cloud assumption in the determination of vertical cloud distribution. According to Wang et al. (2000) who have studied the vertical cloud structures using rawinsonde data, surface observations, and satellite data, the frequency of multilayer clouds occur at about 40% over the globe. Specifically, the frequency of two-layer clouds may reach about 10% at high lati-

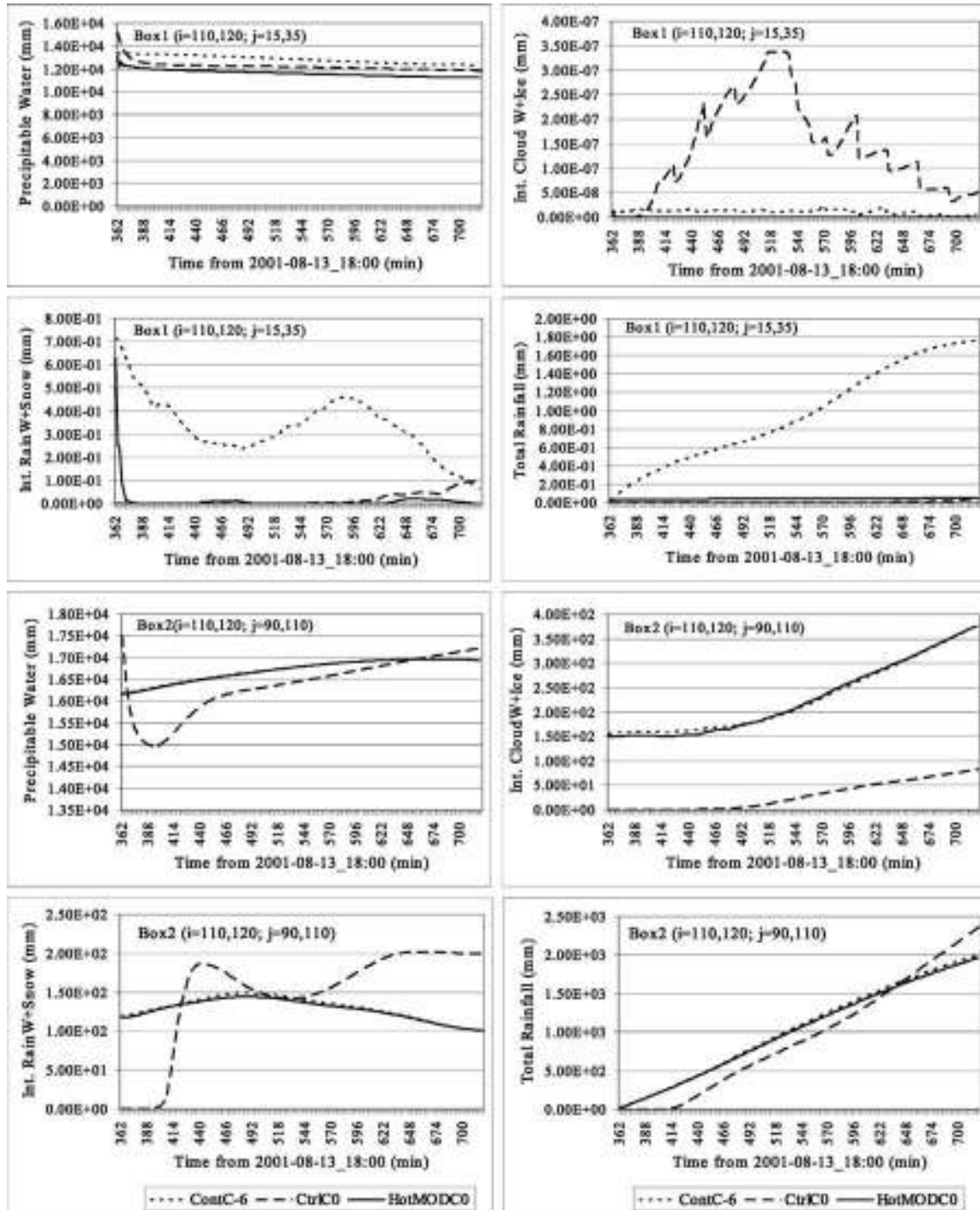


FIG. 1. (left) Total model precipitable water and column-integrated precipitation mass (cloud rain and snow), and (right) rainfall and column-integrated cloud water and ice, within (top two panels) Box1 and (bottom two panels) Box2 shown in Fig. 4 from three model runs of ContC-6 (continuous run starts 6 h earlier than the other two), CtrlC0 (model starts from 6 h later than ContC-6), and HotMODC0 (based on the model state of ContC-6 at 360 min, MODIS data are ingested). Model domain setup and case description can be found in section 2 of text.

tudes. Therefore, the one-layer cloud assumption is not always optimal.

For polar regions, additional data sources from satellite observations are available such as the MODIS instruments on board the National Aeronautics and Space Administration (NASA) Earth Observing System (EOS) satellites *Terra* and *Aqua* (e.g., Key et al. 2003). MODIS level-2 data are now available at 5×5 1-km pixel resolution (i.e., 5-km resolution) on 20 vertical pressure levels (Menzel et al. 2002). The MODIS data validation is conducted by comparing results to in situ radiosonde measurements, the National Oceanic and Atmospheric Administration (NOAA) High-Resolution Infrared Radiation Sounder (HIRS) operational retrievals, GOES sounder operational retrievals, the National Centers for Environmental Prediction (NCEP) analyses, and retrievals from the Atmospheric Infrared Sounder (AIRS)/Advanced Microwave Sounding Unit-A (AMSU-A)/Humidity Sounder for Brazil (HSB) instrument package on the *Aqua* platform; data quality control consists of manual and automatic inspections, with regional and global mean temperatures at 300, 500, and 700 hPa monitored weekly, along with 700-hPa dewpoint temperatures (Menzel et al. 1997; Menzel et al. 2002; King et al. 2003).

As such, the time is now ripe to investigate the following: 1) the degree to which accurate moisture fields for MM5 simulations can be obtained through the utilization/assimilation of humidity profiles retrieved from the MODIS instrument package; 2) the degree to which MODIS-retrieved cloud parameters (e.g., cloud-top temperature, cloud-top pressure) can improve the method for determining vertical cloud distribution used by Fan and Tilley (2002); 3) the feasibility of dynamically ingesting and assimilating the MODIS data during MM5 model integrations through a hot start technique; and 4) the impacts of such a hot start MODIS data assimilation process on high-latitude mesoscale weather prediction. Research along these lines is reported in this paper.

It was noted above that some data assimilation systems are set up in a cyclic mode, where hydrometeor fields from the previous forecast cycle (background) are carried over to the initialization/data assimilation phase for the next forecast cycle. Such a technique can be useful in providing fields for operational systems but with the caveat that new observational data that carries more realistic information (e.g., about cloud hydrometeors) must still be ingested at some point to avoid propagation of model biases from cycle to cycle. As such, the research reported on in this paper still has applications to a cycling system, in that it illustrates

potential benefits of assimilating MODIS data within a cycling system as a means of controlling model biases.

The paper focuses on three specific case study periods: 1) a period during mid-August 2001 characterized by substantial clouds and precipitation over western Alaska and the southern slopes of the Brooks Range (location marked in Fig. 2) stemming from a series of short wave disturbances within a rapid westerly midtropospheric flow; this period was also studied in Fan and Tilley (2002, 2003); 2) the 3-day period of 19–22 July 2002; and 3) the 3-day period of 10–13 February 2003. The first period was studied as a means of formalizing the methodology (sections 2 and 3); results for this period are described in section 4. The second and third periods apply the methodology to MODIS data as described in section 5, via a series of 16 numerical experiments. Results from these test simulation experiments are presented in section 5. Section 6 concludes the study.

2. Preliminary test case and model configuration

a. Preliminary test case

Figure 2 shows the synoptic situation for the 13–16 August 2001 case, as depicted in NCEP–NCAR reanalysis mean 850-hPa geopotential height and cloud cover fields. It is evident that the period was characterized by considerable cloudiness within a propagating westerly flow pattern in the midtroposphere (Fig. 2a). This flow pattern is sustained via the presence of a deep vortex in the western Arctic Ocean and a ridge south of the Alaska Peninsula. Another cyclone is present in the northeast Pacific Ocean. Through the westerly flow pattern, a series of short wave disturbances (as manifested in the series of 1440-m geopotential contours during the period plotted in Fig. 2a) propagated west to east, causing substantial clouds and precipitation over western Alaska and the southern slopes of the Brooks Range. Figure 2b shows the 4-day averaged total cloud fraction in percent; clearly, the cloud coverage pattern reinforces the necessity of performing cloud field initialization and/or assimilation for an accurate representation of the atmospheric state.

The precipitation during this period reflects the fast-moving short wave disturbances. Figure 3 shows the analyzed precipitation, by using the Cressman (1959) interpolation method, from station-observed 1-h precipitation over the Alaska region from 2300 UTC 13 August 2001 to 0200 UTC 14 August 2001.

The coverage of MODIS data (from the *Terra* satellite) at 2210 UTC 13 August and 0000 UTC 14 August 2001 is illustrated in Fig. 4, which depicts the MODIS-retrieved cloud-top temperature fields for these times.

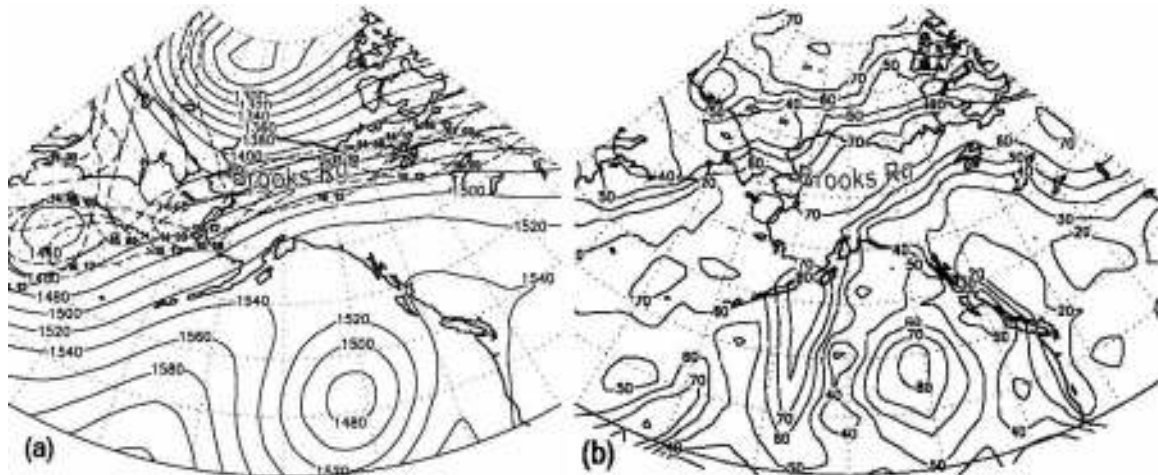


FIG. 2. NCEP-NCAR reanalysis of (a) mean 850-hPa geopotential height (m) and (b) mean total cloud cover (%), averaged over 13–16 Aug 2001. The superimposed dashed contours with date and hour labels (dd_hh) in (a) represent positions of the 1440-m geopotential contour at the indicated time. The location of the Brooks Range is marked in both panels.

Strictly, the MODIS data coverage implied in each panel of Fig. 4 contains four MODIS “granules” (each granule covers 5 min of observation time along the path of the satellite and contains 406×270 5-km cells) observed within 20 min of the specified time. The spatial coverage of the MODIS granules adequately covers our area of interest.

b. Model configuration

To take full advantage of the MODIS data, the MM5 model domain is specified as a 151×205 domain with a 15-km grid spacing, centered at 62.13°N latitude and 154.81°W longitude. Forty-one terrain-following sigma levels are used in the vertical. The standard MM5 model accommodates four-dimensional data assimilation (FDDA) via Newtonian nudging (analysis nudging or observation nudging; Stauffer and Seaman 1990). All the simulations in this study use the Grell (1993) cumulus parameterization and the Reisner et al. (1998) explicit microphysics scheme without graupel. As described by Grell et al. (1994), the Grell cumulus parameterization scheme computes the moisture cycle including downdraft calculations in terms of precipitation efficiency and normalized condensation and precipitation. The Reisner explicit scheme computes tendencies of water vapor, cloud water, cloud ice, snow, and rainwater using cloud microphysics for the auto-conversion, accretion, evaporation, deposition/sublimation, melting, and freezing processes. The Oregon State University (OSU) land surface model (LSM; Chen and Dudhia 2001), Hong and Pan’s (1996) planetary boundary layer (PBL) scheme, and Dudhia’s (1989) two-stream radiative transfer formulation are also used. Ini-

tial atmospheric conditions are obtained from the NCEP-NCAR reanalysis, and are enhanced by surface and upper-air observations through objective analysis using the standard suite of MM5 preprocessing program LITTLE_R (Dudhia et al. 2005). As preliminary results from ongoing work (Tilley et al. 2005), in addition to those presented at a recent high-latitude modeling workshop (see Tilley and Bromwich (2005) for a summary of appropriate workshop papers], do not give a strong advantage to any particular analysis/assimilation methodology with conventional surface and upper-air data, we feel that for the purpose of this study, the utilization of the reanalysis and LITTLE_R methodology described above is adequate.

The initialization time for the preliminary test case is set to 1800 UTC 13 August 2001, and is defined as hour zero (h 0) in the experiments. The simulations run for a 24-h forecast period, with a time step of 40 s.

Since polar-orbiting satellite observation times generally do not conform to hourly periods and can be quite irregular, the model should have the ability to ingest the MODIS data at the time it is observed. For instance, during the first 6-h period of the preliminary test case, there are four MODIS data observation times (1900, 2040, and 2210 UTC 13 August 2001 and 0000 UTC 14 August 2001). A hot start technique has been developed for the MM5 model in order to ingest MODIS data when it is available and has other advantages as well over our previous work. In our previous work, an approximate time range (e.g., ± 30 min) was used to fit the satellite observation time to the model forecast/analysis times; the model was stopped at predetermined forecast times and integration was restarted

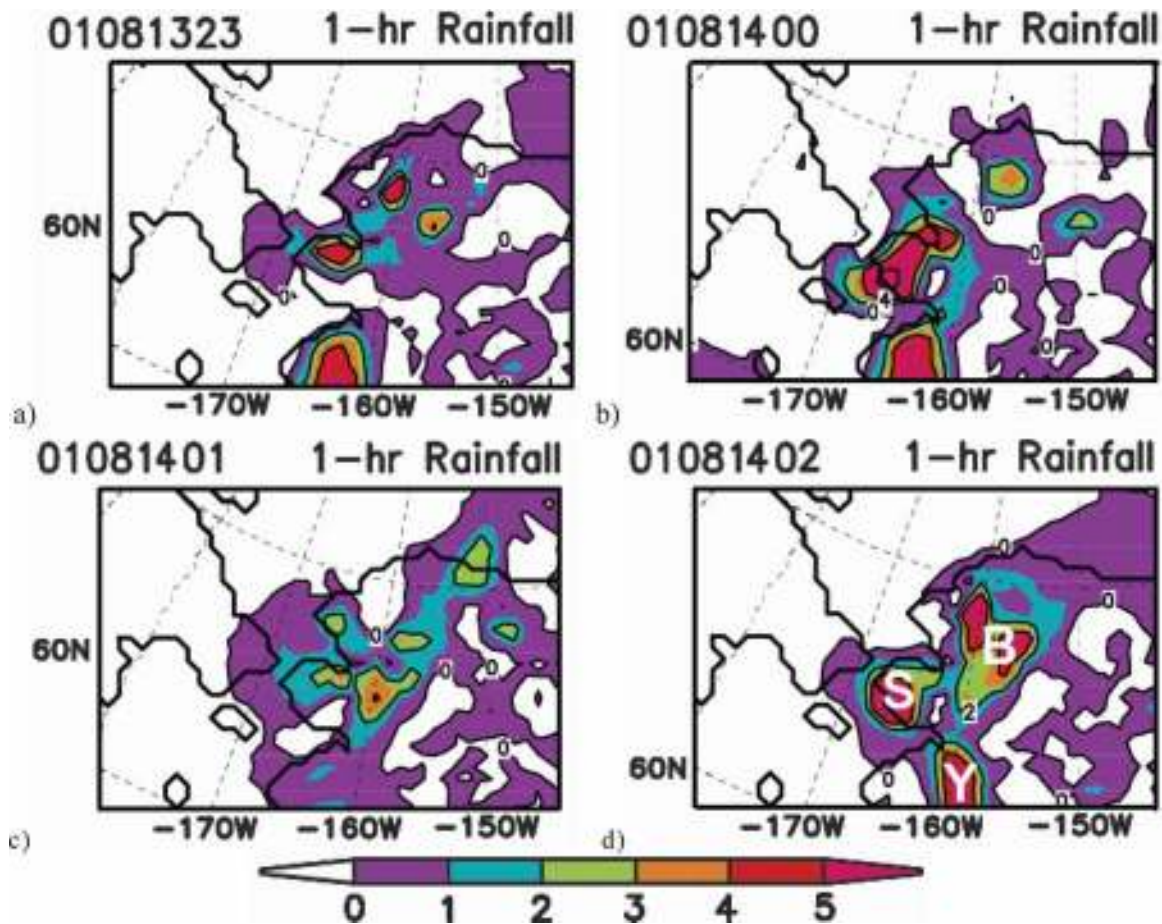


FIG. 3. Analyzed precipitation [interpolated by using Cressman (1959) method] from station observations of 1-h rainfall (mm) for the period 2300 UTC 13 Aug–0200 UTC 14 Aug 2001; letters B, S, and Y in lower right panel indicate the locations of southwest slope of Brooks Range, Seward Peninsula, and the lower Yukon valley, respectively.

as a warm start after the satellite data was assimilated. As such, the spinup process affects the continuity of the model integration. With the hot start technique, all of the model variables at the satellite observation time, except the ones that have been changed from assimilation of the satellite data (described more fully below) will retain the values they had before the assimilation process. In this study, only the water vapor mixing ratio (Q) in the MM5 model will be adjusted during the hot start process, according to the cloud distribution and determination of relative humidity adjustment.

3. Derivation of humidity profiles using MODIS products

The success of the cloud initialization for this study depends on the accuracy of the initial water vapor content. Many studies about cloud prediction and detection, and the relationship of cloud and humidity, especially relative humidity, have been accomplished (e.g.,

Wang et al. 2000; Garand and Nadon 1998; Xu and Randall 1996; Peixoto and Oort 1992, 1996; Lazarus et al. 1999; Haag et al. 2003; Strom et al. 2003; Yi et al. 2004). However, the cloud has been the predictand (i.e., a dependent variable) in all those previous studies. Given the satellite data, it is now practical to utilize the satellite-observed cloud information in numerical modeling.

MODIS level-2 data provides retrieved atmospheric moisture (i.e., dewpoint temperature) and temperature profiles in cloud-free areas; these cloud-free profiles are utilized in this study. After they are interpolated to the MM5 15-km horizontal grid and the 41 vertical sigma levels, these retrieved MODIS humidity profiles are incorporated directly where it is clear.

For cloudy areas, MODIS provides information on cloud-top temperature and cloud-top pressure. Fan and Tilley (2002, 2003) have used a set of empirically derived relative humidity thresholds to infer the relative

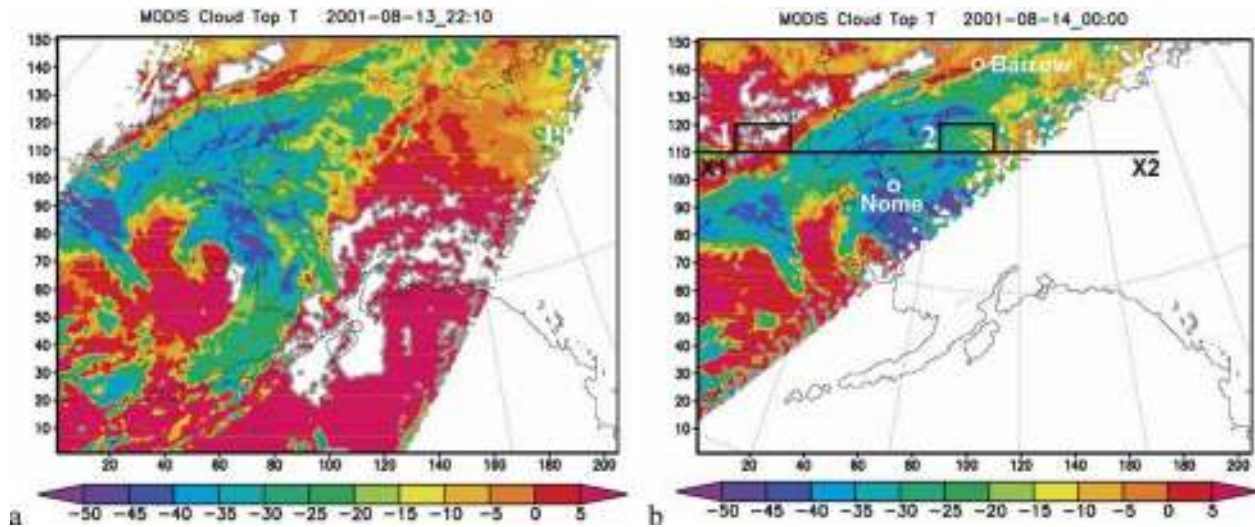


FIG. 4. MODIS-retrieved cloud-top temperature ($^{\circ}\text{C}$) at (a) 2210 UTC 13 Aug and (b) 0000 UTC 14 Aug 2001, interpolated to the MM5 15-km grid used in this study; gray colors indicate missing data. Line X1–X2 denotes the cross section to be shown in Figs. 10 and 14. Two stations marked in (b) are Barrow and Nome, AK. Boxes 1 and 2 indicate the subdomain within which the total values are summed.

humidity inside and outside clouds, once the cloud top and base is determined. The methods for determining the cloud top and base from MODIS observations and MM5 model analyses/forecasts and for adjusting model humidity field are explained below in this section.

The relative humidity thresholds include two critical values for cloudy and clear conditions at a given sigma level, designated as RH_{cld} and RH_{clr} , respectively. If it is cloudy, the relative humidity should be greater than RH_{cld} , and if it is clear, the relative humidity should be less than RH_{clr} . These thresholds are first taken from a climatic analysis of upper-air observations. For example, Fig. 5 shows vertical profiles (1000–100 hPa) of mean relative humidity for 10 cloud types during the Tropical Ocean Global Atmosphere Coupled Ocean–Atmosphere Response Experiment (TOGA COARE; Wang and Curry 1998). Then these thresholds are tuned according to model produced cloud-top distribution and relative humidity, which are validated with satellite cloud images and analysis data. Table 1 gives the final thresholds that are used in this study.

The results from Fan and Tilley (2002) have shown that the MM5 can produce more realistic cloud cover when the adjusted humidity fields are used. However, as a single cloud layer was assumed, in Fan and Tilley (2002), input into the vertical cloud distribution was not always optimal. Similar results were found by Yucel et al. (2002, 2003) regarding the assumption of a single-layer cloud. Clearly, the MM5-generated vertical profiles of temperature, pressure, and winds contain valuable information too. Because of their three-dimen-

sional balance and consistency with respect to the moisture fields, the model humidity, in tandem with the satellite retrievals, is also used to improve the determination of the vertical cloud distribution. The shortcomings caused by the lack of vertical structure details in satellite retrievals at cloudy grid points and the inevitable retrieval errors may be offset by the model information. Therefore, in this paper, both the MM5-analyzed hu-

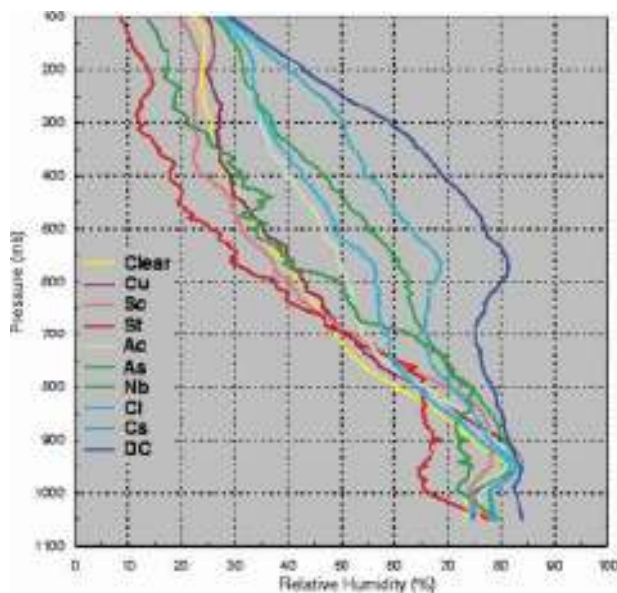


FIG. 5. Vertical profiles (1000–100 mb) of mean RH (%) for 10 cloud types during TOGA COARE. Values at 1050 mb represent surface values (from Wang and Curry 1998).

TABLE 1. The RH (%) thresholds at different sigma levels for both cloud and clear conditions (adopted from Fan and Tilley 2002).

Level No. (σ)	RH _{cl}	RH _{clr}	Level No. (σ)	RH _{cl}	RH _{clr}
1 (0.0090)	85.0	55.0	22 (0.6065)	94.4	77.0
2 (0.0290)	85.5	56.1	23 (0.6385)	94.7	77.9
3 (0.0500)	86.0	57.2	24 (0.6705)	95.0	78.8
4 (0.0725)	86.5	58.3	25 (0.7025)	95.3	79.7
5 (0.0960)	87.0	59.4	26 (0.7335)	95.6	80.6
6 (0.1205)	87.5	60.5	27 (0.7635)	95.9	81.5
7 (0.1460)	88.0	61.6	28 (0.7920)	96.2	82.4
8 (0.1725)	88.5	62.7	29 (0.8190)	96.5	83.3
9 (0.2000)	89.0	63.8	30 (0.8435)	96.8	84.2
10 (0.2285)	89.5	64.9	31 (0.8665)	97.0	85.0
11 (0.2580)	90.0	66.0	32 (0.8875)	97.2	85.8
12 (0.2880)	90.5	67.1	33 (0.9070)	97.4	86.6
13 (0.3190)	91.0	68.2	34 (0.9245)	97.6	87.4
14 (0.3505)	91.4	69.2	35 (0.9405)	97.8	88.2
15 (0.3825)	91.8	70.2	36 (0.9550)	98.0	89.0
16 (0.4145)	92.2	71.2	37 (0.9680)	97.5	89.1
17 (0.4465)	92.6	72.2	38 (0.9790)	97.0	89.2
18 (0.4785)	93.0	73.2	39 (0.9875)	96.5	89.3
19 (0.5105)	93.4	74.2	40 (0.9935)	96.0	89.4
20 (0.5425)	93.8	75.2	41 (0.9975)	95.0	89.0
21 (0.5745)	94.1	76.1			

midity profile and the relative humidity thresholds are used in order that a vertical humidity structure similar to the MM5 analysis is obtained while the adjusted humidity fields also tend to produce more realistic cloud fields. We describe the procedures to determine cloud top and base and to adjust the model humidity in the following subsections.

a. Cloud top and base

Figure 6 shows a flowchart for determination of cloud top and base using MODIS-retrieved cloud-top temperature, cloud-top pressure, and MM5 analysis/forecast fields.

As for all remotely sensed fields, MODIS-retrieved products contain errors. Menzel et al. (2002) reported that the maximum error for MODIS cloud-top pressure (denoted here by CTP_{err}) is about 100 hPa while the maximum error for temperature profiles (denoted here by CTT_{err}) is about 2 K. Using the MM5 temperature profile, the model cloud top is considered present at the sigma level where the model temperature equals to the MODIS cloud-top temperature (CTT), denote the cloud-top level determined by CTT as K_t . Multiple K_t is possible in cases of temperature inversions. Similarly, the cloud-top sigma-level index determined by MODIS cloud-top pressure (CTP) is denoted as K_p . Because of the errors in CTT and CTP, a consistency check is per-

formed between the K_t and K_p in order to obtain an optimal cloud-top level (denoted as K_{tp}) determined from MODIS CTT and CTP. If no K_t or K_p is found, it means no cloud; K_{tp} is set to a sentinel value of -1 . If no K_t but K_p is found, then $K_{tp} = K_p$. If no K_p but K_t are found, then we use the highest K_t as K_{tp} . If K_t equals to K_p , they are consistent and $K_{tp} = K_t = K_p$. In all other cases when both K_p and K_t are found but not consistent, we choose the closest K_t to K_p and then check on the difference between K_t and K_p . If there is only one level difference, we choose the one that has less error. If $[|P(K_p) - CTP|/CTP_{err}] > [|T(K_t) - CTT|/CTT_{err}]$, $K_{tp} = K_p$, otherwise, $K_{tp} = K_t$. If the difference between K_t and K_p is two levels, then we average them and $K_{tp} = (K_t + K_p)/2$. If the difference is more than two levels, we choose the level K_i between K_t and K_p for K_{tp} , which minimizes the absolute difference $[|P(K_p) - P(K_i)|/CTP_{err}] - [|T(K_t) - T(K_i)|/CTT_{err}]$.

As mentioned above, MM5 humidity profiles are also used so that the MODIS observations and MM5 fields are combined in determining the cloud top, and in representing multilayer clouds as well (see the humidity adjustment procedures below). First, the MM5 relative humidity profiles and RH_{cl} are used to find the MM5 analysis/forecast-suggested cloud-top level. When searching downward from model top, the model-suggested cloud top, denoted as K_{mct} , is the first level encountered where $RH(K_{mct}) > RH_{cl}$. If no level is found that the relative humidity is greater than the level's RH_{cl}, it is clear and $K_{mct} = -1$. If either $K_{tp} = -1$ or $K_{mct} = -1$ is the case, the final cloud top K_{top} is set to K_{tp} . In cases that both satellite and MM5 analysis/forecast indicates cloud existence ($K_{tp} > 0$ and $K_{mct} > 0$), if either pressure or temperature difference between levels K_{tp} and K_{mct} are less than MODIS errors CTP_{err} or CTT_{err}, respectively, the model cloud level K_{mct} is used (i.e., $K_{top} = K_{mct}$). Otherwise, the midpressure level between $P(K_{tp})$ and $P(K_{mct})$, $P = [P(K_{tp}) + P(K_{mct})]/2$, is assigned to be the final cloud top.

Determination of cloud base follows Fan and Tilley (2002) with reference to the cloud detection algorithm of Garand and Nadon (1998). Considering the lifting condensation height, cloud base is considered at a level where the temperature is colder than surface temperature (T_s) by 3–6 K (Garand and Nadon 1998). However, there often exist temperature inversions at high latitudes. For example, from a statistical study at the time 0000 UTC 14 August 2001 for the whole model domain within the troposphere, temperature inversions occur at about 20% out of total 30 955 grid points, wherein 4.7% grid points have more than one inversion. In such instances, there may be levels where the temperature is

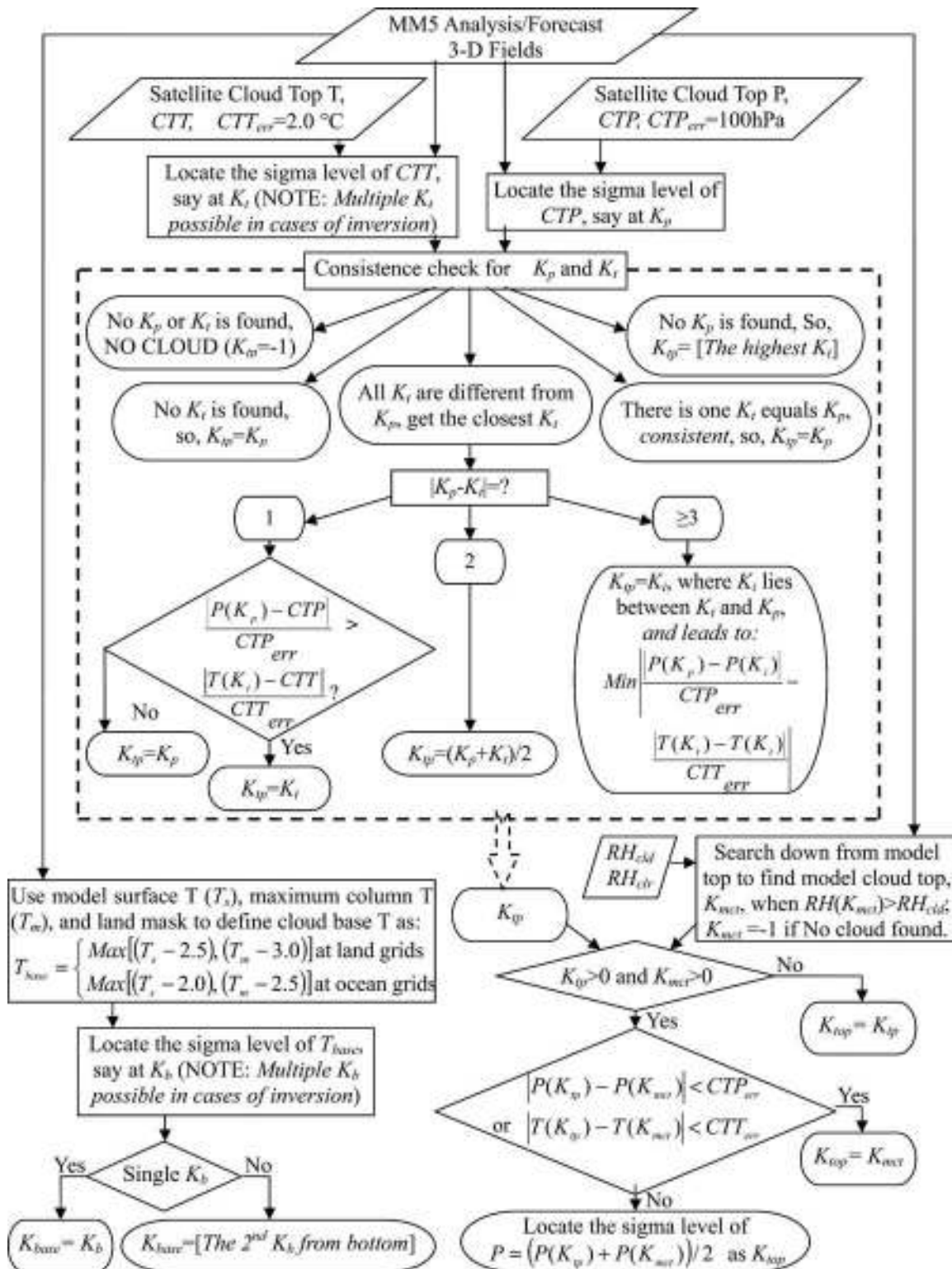


FIG. 6. Flowchart for determination of cloud top and base.

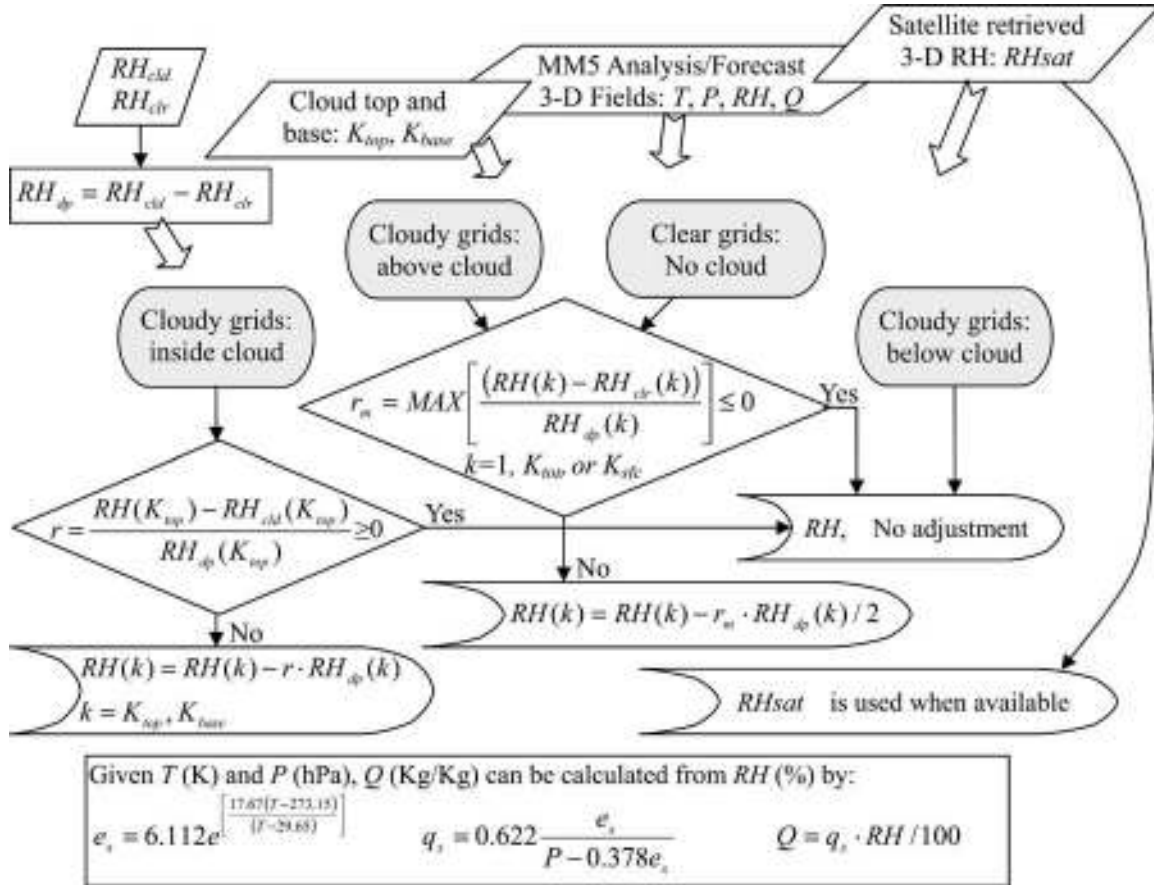


FIG. 7. Flowchart for humidity adjustment.

warmer than the surface temperature. Thus, the maximum temperature of a vertical column (T_m) is also used. By comparing to sounding observations and being tested in the model, the cloud-base temperature (T_{base}) is designed in this study as the larger of ($T_s - 2$) and ($T_m - 2.5$) for ocean grid points, the larger of ($T_g - 2.5$) and ($T_m - 3$) for land grid points. By searching from the surface upward to compare T_{base} and model temperature, the cloud-base level is located at the sigma level where the model temperature equals T_{base} . Again, multiple K_b is possible in cases of inversions. If only one K_b is found, then the final cloud-base level is $K_{base} = K_b$. If more than one K_b is found, the second K_b from bottom is identified as K_{base} . The rationale for this is that when a single inversion (more likely radiation inversions) is present at lower levels, the profile is statically stable below the inversion. The situation differs when there is more than one solution, the layer above the first inversion may be unstable where cloud formation may occur.

If the detected cloud-top level is lower than cloud-base level, it is declared clear (no cloud). This happens when MODIS observes only thin low clouds.

b. Humidity

Once the cloud top and cloud base are determined, the humidity for cloudy grid points is obtained by utilizing the relative humidity thresholds and referencing the MM5-analyzed or -forecasted humidity profile. The difference between the two thresholds for cloudy and clear conditions at each level, $RH_{dp} = RH_{cld} - RH_{clr}$, is used as a measuring scale of dry or wet extent. Figure 7 shows a flowchart for model humidity adjustment.

To use the original MM5-analyzed/forecasted vertical cloud distribution as a prototype of multilayer clouds, model humidity profile inside the cloud is adjusted columnwise according to humidity at cloud top. If the relative humidity at the cloud-top level is equal to or greater than this level's RH_{cld} (i.e., if $r = [RH(K_{top}) - RH_{cld}(K_{top})] / RH_{dp}(K_{top}) \geq 0$), no adjustment is needed. Otherwise, an adjustment is made as

$$RH(k) = RH(k) - rRH_{dp}(k), \quad k = K_{top} \dots, K_{base}. \quad (1)$$

For clear grid points where there is no cloud, and at levels above the cloud top for cloudy grid points, the

TABLE 2. Characteristics of experiments described in this paper.

No.	Expts Name	Description			
		Initial time (UTC and date)	Total time	Analysis nudging	MODIS data
1	iCtrl	0000 14 Aug 2001	18 h	No	No
2	iMODIS	0000 14 Aug 2001	18 h	No	Yes, initial time at 0000 UTC 14 Aug
3	Ctrl	1800 13 Aug 2001	24 h	No	No
4	hotMODIS	1800 13 Aug 2001	24 h	No	Yes, 4 times at 1900, 2040, 2210 UTC 13 Aug and 0000 UTC 14 Aug
5	Ctrlfdda	1800 13 Aug 2001	24 h	0–6 h	No
6	hotMODISfdda	1800 13 Aug 2001	24 h	0–6 h	Yes, 4 times at 1900, 2040, 2210 UTC 13 Aug and 0000 UTC 14 Aug

maximum wet extent measure with regard to the clear condition relative humidity threshold is calculated by

$$r_m = \text{Max} \left[\frac{\text{RH}(k) - \text{RH}_{\text{clr}}(k)}{\text{RH}_{\text{dp}}(k)} \right],$$

$$\begin{cases} k = 1 \dots, K_{\text{top}} & \text{aboveCloudTop} \\ k = 1 \dots, K_{\text{sfc}} & \text{clearGrids} \end{cases} \quad (2)$$

If $r_m \leq 0$, even the wettest level is already dry and clear, so no adjustment is needed. If $r_m > 0$, an adjustment is made as

$$\text{RH}(k) = \text{RH}(k) - r_m \text{RH}_{\text{dp}}(k)/2,$$

$$k = 1 \dots, K_{\text{top}} \text{ or } K_{\text{base}}. \quad (3)$$

The ratios r and r_m in Eqs. (1)–(3) make it possible to adjust model humidity columnwise, and the adjustment is likely a translation of the MM5-analyzed/forecasted humidity profile; thus, if available, the model multilayer cloud pattern can be retained. In Eq. (3), a factor of 2 is used to avoid overdrying in the adjustment, since the ratio r_m represents the wettest case.

The MM5-analyzed humidity below the cloud-base level is left unchanged. Since the cloud base is determined with the model surface temperature and the column maximum temperature has already been used, no more adjustment is necessary for the model humidity fields below cloud base. However, for consistency, all the MODIS-retrieved relative humidity is used where it is available.

Actually, the water vapor mixing ratio (Q) is the humidity variable used within both the MM5 initialization procedure and the forecast model. As such, once the new adjusted relative humidity field is obtained, the values of relative humidity are converted to mixing ratios for use in the MM5; assuming constant temperature when performing the conversions implies:

$$Q = q_s \text{RH}/100, \quad (4)$$

$$q_s = 0.622 \frac{e_s}{P - 0.378e_s} \quad \text{and}$$

$$e_s = 6.112e^{[17.67(T-273.15)/(T-29.65)]}. \quad (5)$$

4. Numerical experiments and results

The experiments conducted for the August 2001 test period are listed in Table 2. Experiment Ctrl is the standard MM5 starting from hour 0 without FDDA, while experiment Ctrlfdda is the standard MM5 run with analysis nudging during hours 0–6. Experiments iCtrl and iMODIS are conducted to examine the impacts of MODIS data when this data are assimilated at the initial time, 0000 UTC 14 August 2001, only. The initial time chosen for this event is due to the good satellite data coverage at this time. Experiments hotMODIS and hotMODISfdda use the hot start technique to dynamically ingest MODIS data when it is available during the full assimilation period (i.e., hours 0–6), and should be considered as parallel experiments to experiments Ctrl and Ctrlfdda, respectively.

a. Model relative humidity adjustment and results

As described above, the MODIS data are assimilated to modify the model humidity field, specifically, the water vapor mixing ratio in the MM5. In this section, we examine the changes of the model water vapor and relative humidity when the MODIS data are assimilated via the hot start technique from experiment hotMODIS. In experiment hotMODIS, MODIS data from three satellite passes (i.e., 1900, 2040, and 2210 UTC 13 August 2001) prior to 0000 UTC 14 August 2001 (a fourth satellite pass) have been assimilated into MM5. After the data of this fourth satellite pass are assimilated, the simulation continues as a “free fore-

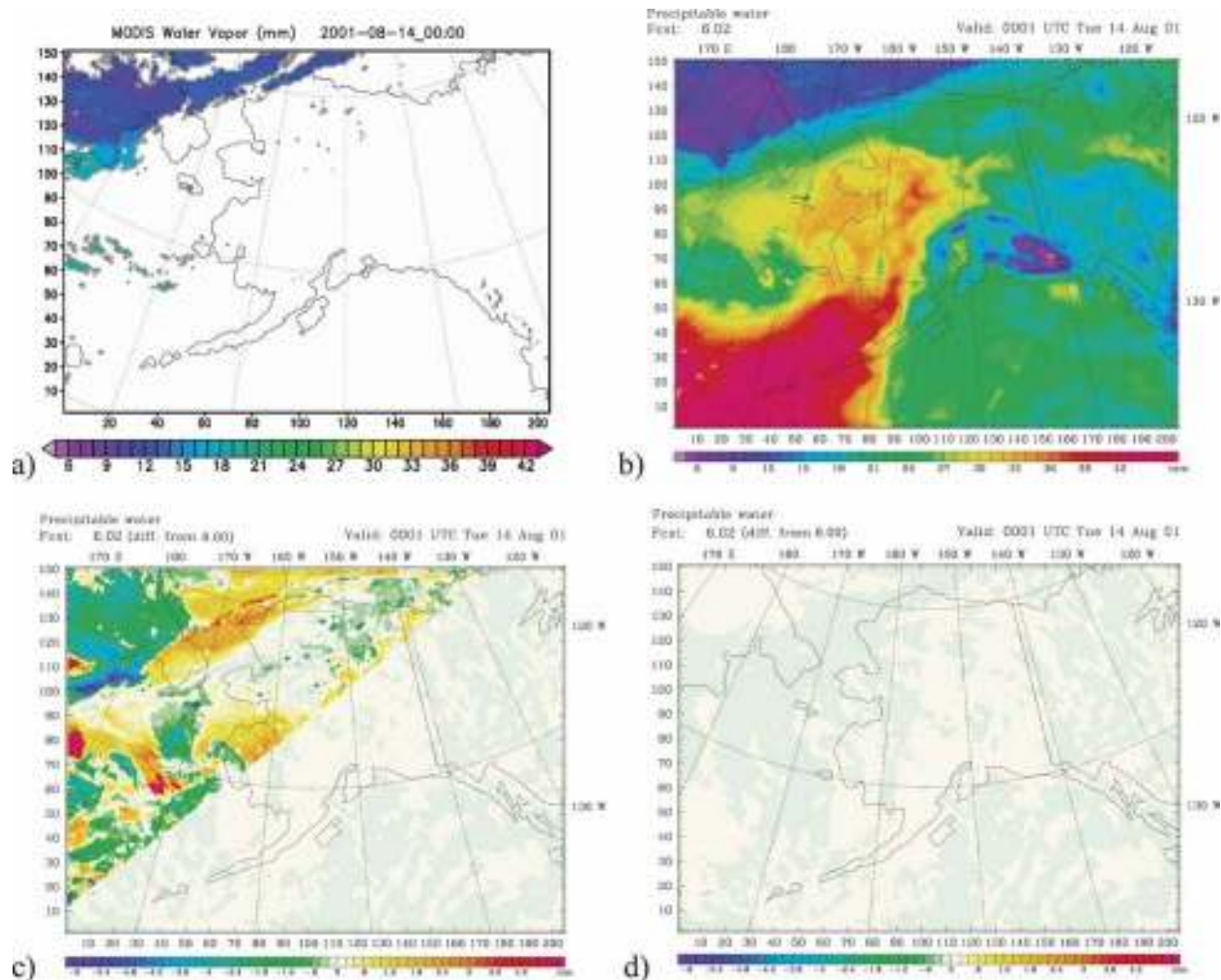


FIG. 8. (a) MODIS-retrieved total water vapor (mm) at 0000 UTC 14 Aug 2001 (model forecast hour 6); (b) model precipitable water (column-integrated water vapor, mm) from experiment hotMODIS at model forecast hour 6.02, which is two time steps (80 s) after the MODIS data are assimilated; (c) precipitable water difference of hour 6.02 from hour 6 (MODIS data are not assimilated yet at hour 6) in experiment hotMODIS; (d) precipitable water difference of hour 6.02 from hour 6 from a hotMODIS run without the MODIS data at 0000 UTC 14 Aug 2001 assimilated.

cast.” This time (0000 UTC 14 August 2001) is chosen to illustrate the change in the MM5 model humidity fields resulting from the ingestion of MODIS data within the dynamic assimilation cycles.

For testing how the model water vapor is changed during the hot start assimilation, a parallel model experiment is conducted and compared to experiment hotMODIS. At model forecast hour 6 (i.e., 0000 UTC 14 August 2001), the hotMODIS output, which does not contain impacts from the MODIS data at the same time, is used as a baseline for the test. Then we continue the model run and output at every time step. The parallel model run is the same as hotMODIS except the MODIS data at 0000 UTC 14 August 2001 is not assimilated. Figure 8 shows the model results of column-

integrated water vapor from the MODIS data assimilation and humidity adjustment. Figure 8a shows the MODIS-retrieved total water vapor that is only available at clear grids. Figure 8b shows the model precipitable water (column-integrated water vapor) from experiment hotMODIS at model forecast hour 6.02, which is two time steps (80 s) after the MODIS data are assimilated. The spatial distribution of total water vapor is consistent with the MODIS-retrieved water vapor in Fig. 8a. Figure 8c shows the precipitable water difference of hour 6.02 from hour 6 (when the MODIS data are not assimilated yet) in experiment hotMODIS. Figure 8d shows similar results as Fig. 8c but from the parallel run without MODIS data assimilated. From Fig. 8c, the model water vapor is changed

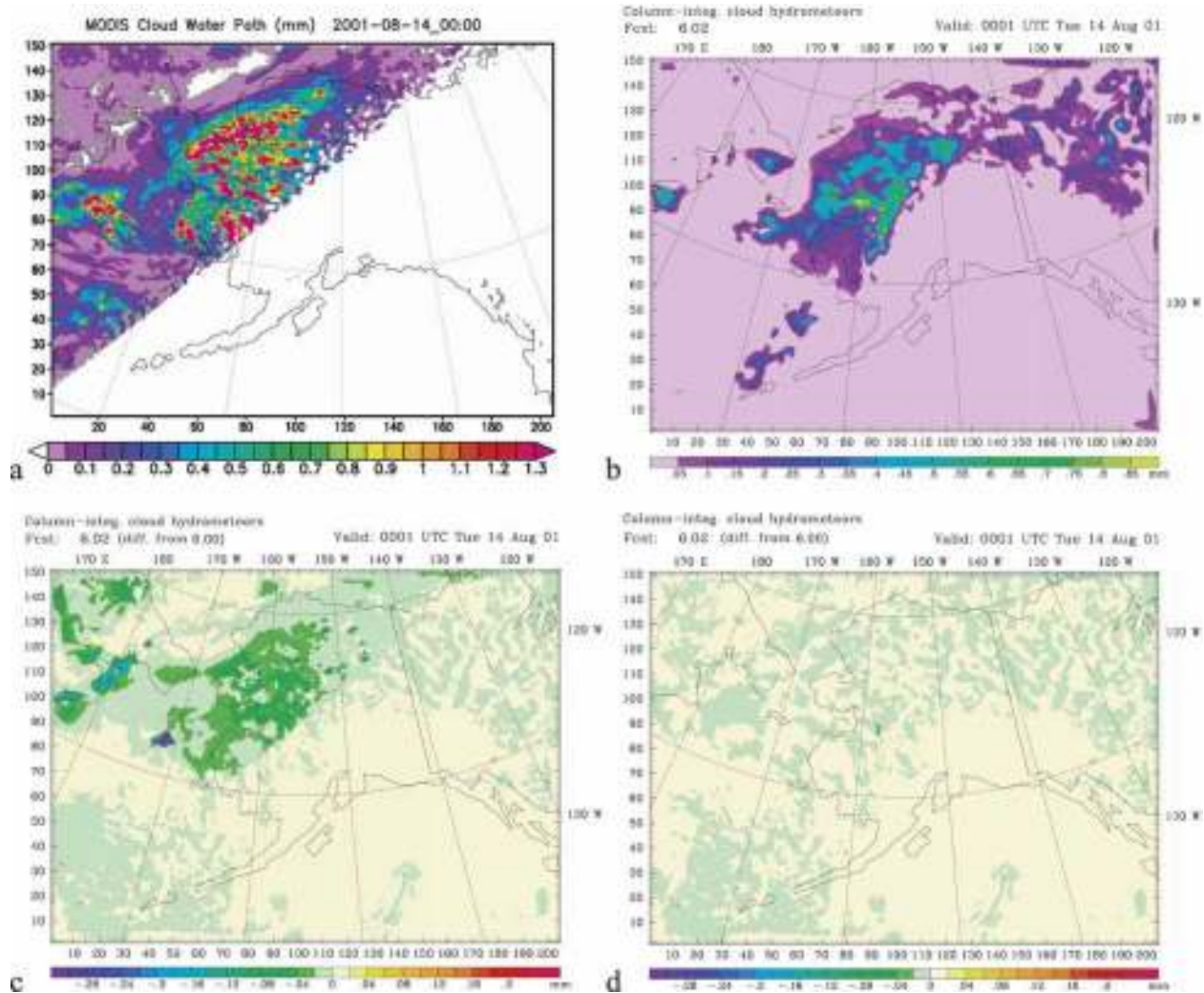


FIG. 9. Same as in Fig. 8 but for cloud water path: (a) MODIS-retrieved cloud water path (mm) at 0000 UTC 14 Aug 2001 (model forecast hour 6); (b) model column-integrated cloud water and ice (mm) from experiment hotMODIS at model forecast hour 6.02, which is two time steps (80 s) after the MODIS data are assimilated; (c) difference of column-integrated cloud water and ice of hour 6.02 from hour 6 (MODIS data are not assimilated yet at hour 6) in experiment hotMODIS; (d) difference of column-integrated cloud water and ice of hour 6.02 from hour 6 from a hotMODIS run without the MODIS data at 00 UTC 14 Aug 2001 assimilated.

as the MODIS data are assimilated. It is obvious that the water vapor is increased in cloudy areas and decreased in clear areas, in comparing the MODIS clouds shown in Fig. 4b. Figure 8d indicates that the changes shown in Fig. 8c is caused from the MODIS data assimilation since the changes from model evolution is very small (Fig. 8d).

Figure 9 shows similar experiments and results as in Fig. 8 but is for cloud water path, which is equivalent to column-integrated cloud water and ice. It is shown that model has smaller magnitude in column-integrated cloud mass (Fig. 9b) compared to MODIS retrievals (Fig. 9a). Figure 9c indicates that the impacts of MODIS data assimilation on model clouds start right

after the model water vapor mixing ratio is modified. Again, the influences from MODIS data are larger than the model evolution itself by considering Fig. 9d.

The impacts on the model relative humidity are also studied within experiment hotMODIS. Figure 10 shows, the adjustment of relative humidity on a cross section (X1–X2 in Fig. 4b) at the exact time when the fourth pass of MODIS data are ingested. Specifically, Fig. 10a shows the relative humidity before and, in Fig. 10b, after the ingestion of MODIS data at 0000 UTC 14 August 2001.

The relative humidity in Fig. 10a contains the cumulative impact from ingesting the previous three passes of MODIS data, while the relative humidity in Fig. 10b

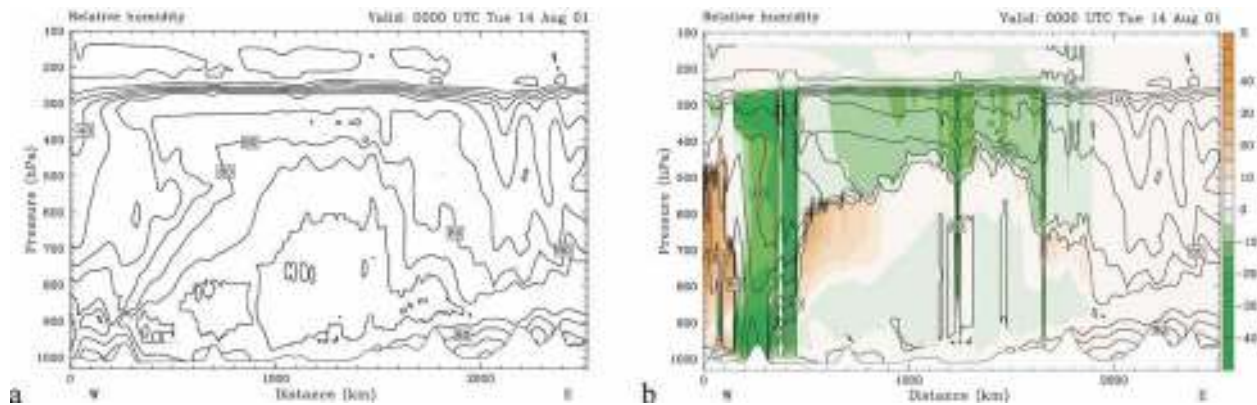


FIG. 10. Relative humidity (%) along cross section (X1–X2 in Fig. 4b) at 0000 UTC 14 Aug 2001 for experiment hotMODIS: (a) before the MODIS data are ingested; (b) after the MODIS data are ingested; in (b) the difference from (a) is shaded.

shows the additional impact from the fourth pass of MODIS data. From Fig. 10b, it is apparent that there are large areas of reduced relative humidity above the cloud top and over clear areas. In addition, increased relative humidity appears within the cloud layer. The maximum relative humidity adjustment has a magnitude of approximately $\pm 50\%$. Large horizontal gradients of relative humidity are found in columns between clear skies (or very low cloud) and cloudy skies in reference to Fig. 4b. These changes demonstrate that the satellite-observed cloud distribution is reflected within the adjusted relative humidity field. Since the model analyzed/forecasted humidity profiles were taken into account in the hot start technique, the adjusted relative humidity did not show any disturbance at the data edge area, as illustrated in Fig. 10b at about a 1900-km distance to the western boundary.

To further investigate the relative humidity changes, Fig. 11 gives the relative humidity profiles before and after the MODIS data are ingested for two stations, Nome and Barrow, Alaska (locations shown in Fig. 4b). From Fig. 4b, it is clear in Barrow and cloudy in Nome at the time 0000 UTC 14 August 2001. The observed relative humidity profiles are also shown in Fig. 11. For the Barrow station, the original model relative humidity is closer to the observation. The MODIS retrievals are available for this station, so the adjusted relative humidity reflects the MODIS-retrieved results. Both MM5 forecast and MODIS retrieval show a dry bias in upper levels and a wet bias in lower levels. One reason why the MM5 did not catch the observed profiles is that the model used less vertical levels than the observations. Similarly, the MODIS retrievals have even fewer levels than the MM5 model. For the Nome station, the same biases are shown for MM5. However, after the MODIS data are ingested, the model cloud top is raised.

b. Impacts of MODIS data assimilation on model clouds

To investigate the impacts of MODIS data assimilation on model clouds, we examine experiment iMODIS, for which MODIS data are ingested only at the initial time (i.e., hour 0, 0000 UTC 14 August 2001) in the simulation. To examine this impact, we have computed the *relative* root-mean-square differences (rmsds) of the temperature and hydrometeor (i.e., water vapor, cloud water, cloud ice, cloud rain, and cloud snow) mixing ratios between the parallel experiments iMODIS and iCtrl for the whole domain at each sigma level. Domain-averaged relative rmsd results for these fields are

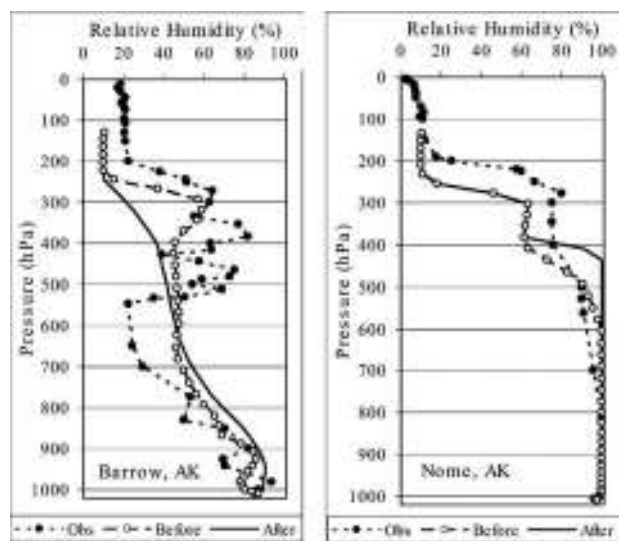


FIG. 11. Relative humidity profiles at two stations, (left) Barrow and (right) Nome, AK (locations are shown in Fig. 4b). Dotted lines are rawinsonde observed profiles; dashed and solid lines are profiles before and after the adjustment, respectively, in the model at the closest grid point to each station.

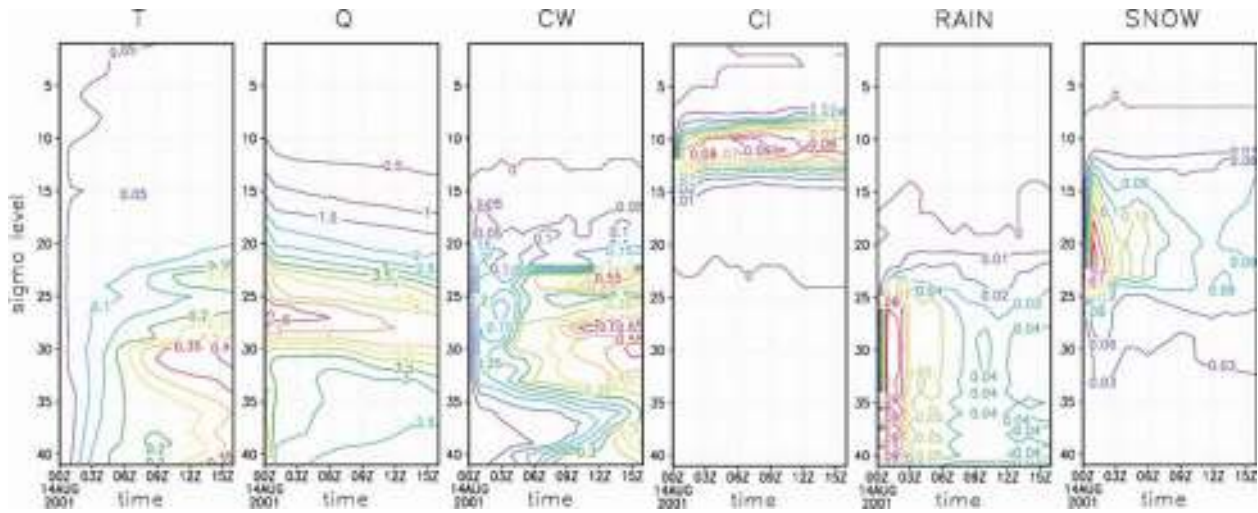


FIG. 12. Time-height sections of domain-averaged *relative rmsds* between experiments iMODIS and iCtrl for (left to right) the variables T (K), Q (g kg^{-1}), CW (cloud water mixing ratio) (g kg^{-1}); CI (cloud ice mixing ratio) (g kg^{-1}); RAIN (rain mixing ratio) (g kg^{-1}); and SNOW (snow mixing ratio) (g kg^{-1}).

illustrated in Fig. 12. From a microphysical viewpoint, immediate impacts on water vapor are indicated at the initial time when the MODIS data are ingested. This is the expected result in terms of the hot start motivation. As the model evolves, balances between temperature and cloud hydrometeor fields are thermodynamically maintained by microphysical processes. The impacts of MODIS data ingestion on cloud ice, rainwater, and snow are shown shortly after the initial time. Long-term impacts on temperature, water vapor, cloud water, and cloud ice are also reflected from the large relative rmsd areas extending along the time axis. These results indicate that the assimilation of MODIS-retrieved humidity impacts model cloud hydrometeor fields and consequently the model cloud distribution. These modifications are further discussed next from a macroscopic viewpoint.

As Fig. 4 shows, the satellite clearly sees the cloud system, though it cannot entirely see all structural elements in a multilayered cloud deck. Similarly, the model does not always present a correct horizontally distributed cloud field compared to that seen from space, especially with respect to mesoscale structure. For example, consider Fig. 13, which shows the cloud-top temperature field derived from experiments Ctrl and hotMODIS, at forecast hours 5, 6, and 7. The MODIS data are available at forecast hours 1, 2.67, 4.17, and 6 for experiment hotMODIS. By comparing Figs. 13b,d,f with Figs. 13a,c,e, respectively, it is clear that after the ingestion of MODIS data, considerable mesoscale structure is added to the modeled cloud fields. As another example, consider Fig. 4a, which shows the satellite-observed cloud-top temperature. The figure indi-

cates wisps of high cloudiness where cloud-top temperatures are in the range -40° to -45°C . The Ctrl run cloud-top temperature field (Fig. 13a) shows sheets of high clouds (-40° to -45°C) southwest of the Brooks Range and south of Bering Strait. The hotMODIS run result (Fig. 13b) shows clouds in smaller horizontal clusters, which is more similar to the cloud field depicted by satellite (cf. Fig. 4a). In general (see also Figs. 13c–f), the Ctrl run produced more horizontal cloud cover (in percentage) than observed by satellite, and was not able to resolve high clouds from low clouds in as much detail as possible from the observations. However, after the MODIS data are assimilated, the cloud-top temperature field shows less coverage and some higher horizontal gradients (more distinct high and low cloud areas) in cloud coverage than in the Ctrl run. The impacts of MODIS data on the spatial distribution of cloud cover are shown at 1 (Figs. 13a,b) and 2 h (Figs. 13c,d) after the ingestion of MODIS data observed at 2210 UTC 13 August 2001 (Fig. 4a), and are also shown at 1 h (Figs. 13e,f) after the ingestion of MODIS data at 0000 UTC 14 August 2001 (Fig. 4b).

To illustrate the impacts of this adjustment on clouds, Fig. 14a presents the distribution of model hydrometeor mixing ratios (cloud water, cloud ice, snow, and rain mixing ratios) for experiment hotMODIS at 0200 UTC 14 August 2001 along the same cross section as Fig. 10. Figure 14a shows that the cloud systems have a spatial scale of about 100–200 km, especially the cloud ice field, which generally corresponds to the cloud top as seen from the satellite. The difference fields of the various mixing ratios of hotMODIS minus Ctrl (see Fig. 14b) indicate that, after 2 h of model integration from

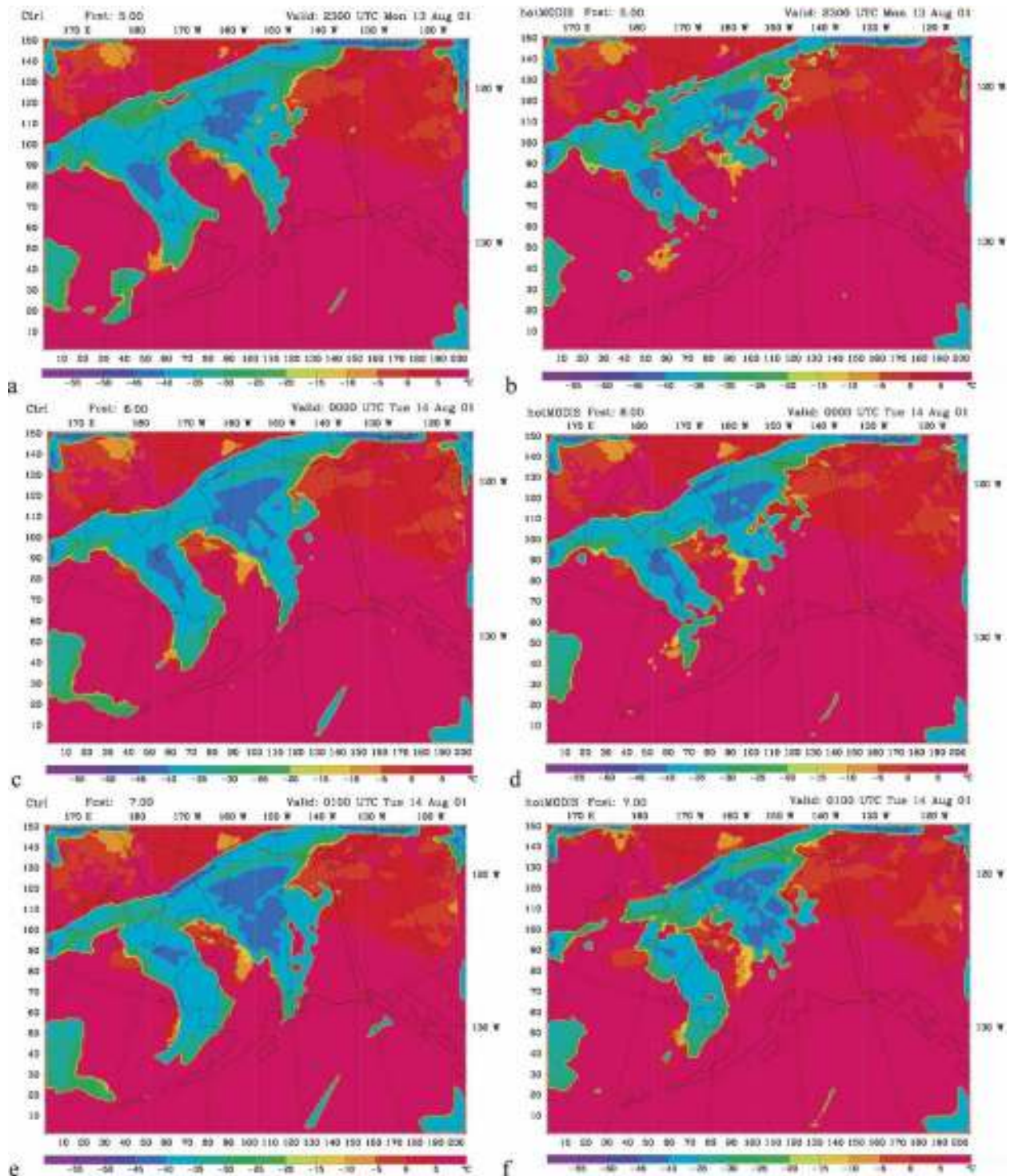


FIG. 13. MM5-derived cloud-top temperature fields ($^{\circ}\text{C}$) at (a), (b) 2300 UTC 13 Aug, (c), (d) 0000 UTC 14 Aug, and (e), (f) 0100 UTC 14 Aug 2001 for (a), (c), (e) experiment Ctrl and (b), (d), (f) experiment hotMODIS, respectively.

the last ingestion of MODIS data, the model cloud fields are changed significantly. Most cloudy areas present in the Ctrl run are still present in experiment hotMODIS, but with reduced cloud hydrometeor mix-

ing ratios. However, there are areas where the simulated cloud mixing ratios are increased in experiment hotMODIS as well. As a result, the mesoscale structure of the cloud field is increased in experiment hotMODIS

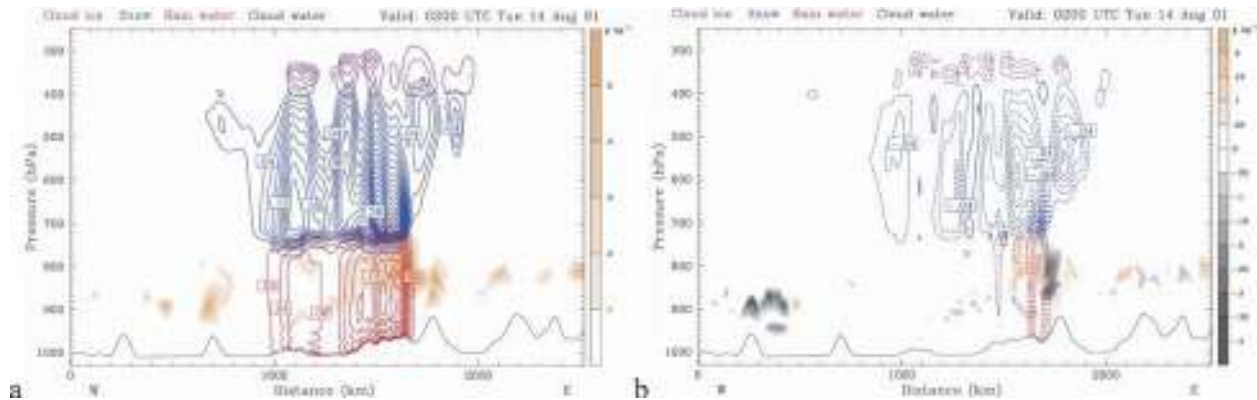


FIG. 14. (a) MM5 mixing ratios (g kg^{-1}) of cloud ice (violet), cloud snow (blue), cloud rain (red), and cloud water (shaded) for experiment hotMODIS along cross section X1–X2, valid at 0200 UTC 14 Aug 2001; (b) difference fields of the mixing ratios in (a), experiment hotMODIS – experiment Ctrl.

compared with the Ctrl experiment. Such an increase in mesoscale structure is similar to that seen above for the horizontal spatial cloud distribution, and suggests that such increase in structure from the application of satellite information occurs over substantial portions of the domain.

c. Precipitation forecast

After the assimilation of satellite data, the model cloud distribution is updated through the adjustment of humidity. The impacts of this adjustment on precipitation and other meteorological fields are discussed in this and the following subsection.

Figure 15 shows the spatial distribution of hourly accumulated precipitation amounts from experiments Ctrl and hotMODIS, for each of the forecast hours 5–8. The hotMODIS forecasts have more mesoscale structure than seen in the Ctrl forecasts. The large areas of precipitation produced in the Ctrl simulation are instead depicted as smaller units within the hotMODIS simulation. Comparison with Fig. 3 shows that most of the smaller precipitation centers seen in the hotMODIS forecasts as well as the spatial gaps between the centers in that simulation correspond to rainfall centers that were observed. In other words, the hotMODIS experiment caught more structural details than the Ctrl experiment. We consider such impacts on the precipitation field a positive feature, which is found as early as 2300 UTC 13 August, within the first hour after the assimilation of MODIS information at 2210 UTC. The figures also show that the precipitation amounts on the Seward Peninsula (indicated by S in Fig. 3d) are more robust in the hotMODIS experiment compared with the Ctrl experiment, though they are not as large as

observed. At the second free forecast hour (0200 UTC 14 August), the observed rainfall has three major maxima, one southwest of the Brooks Range (B in Fig. 3d), one on the Seward Peninsula (S in Fig. 3d), and one in the lower Yukon Valley (Y in Fig. 3d). From Figs. 15g,h, only a small portion of the rain maxima areas S and B are reproduced within the Ctrl experiment, but the hotMODIS experiment produced greater amounts for center S. The rain maximum B was displaced eastward of its observed position in the Ctrl experiment, while in the hotMODIS experiment this area of rain was closer to the observed position, even though still displaced somewhat eastward. Moreover, the large rainfall maximum Y was not produced in either experiment. In both cases, comparison of simulated and observed precipitation trends suggests that the simulated precipitation system translates eastward too rapidly. This problem seems independent from considerations of the humidity field, and is tied more to the mesoscale dynamics operating in both simulations. Adjustment or improvement of other model fields may be a key ingredient toward reducing this propagation error.

Experiment hotMODISfdda, in which other model fields are adjusted with the standard MM5 Newtonian nudging approach, was conducted to examine this hypothesis. Figure 16 shows the same fields as in Fig. 15 for experiment hotMODISfdda. The rain maximum Y, which is incorrectly reproduced in the hotMODIS simulation (cf. Fig. 15) is quite apparent in Fig. 16. In addition, the placement and magnitude of the rain maxima S and B are also improved when nudging is applied together with the assimilation of MODIS data. The difference contours in Fig. 16 show the impacts of MODIS data on the precipitation forecast relative to experiment Ctrlfdda (figure not shown). The MODIS

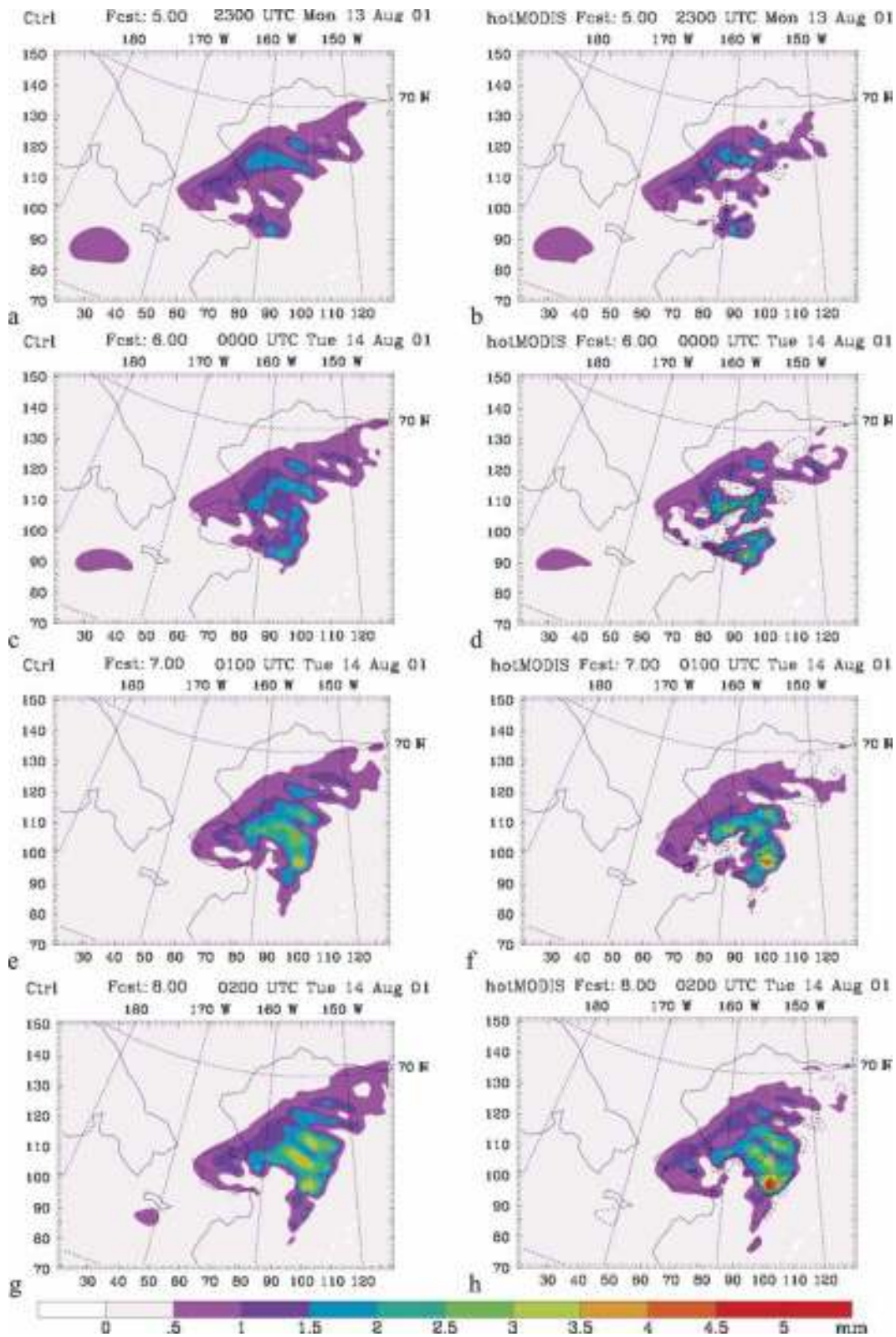


FIG. 15. MM5 1-h accumulated precipitation forecasts (mm; shaded) from experiments (a), (c), (e), (g) Ctrl and (b), (d), (f), (h) hotMODIS at the forecast hours 5-8 (2300 UTC 13 Aug-0200 UTC 14 Aug 2001). Contours in (b), (d), (f), and (h) show the precipitation difference (mm), hotMODIS - Ctrl.

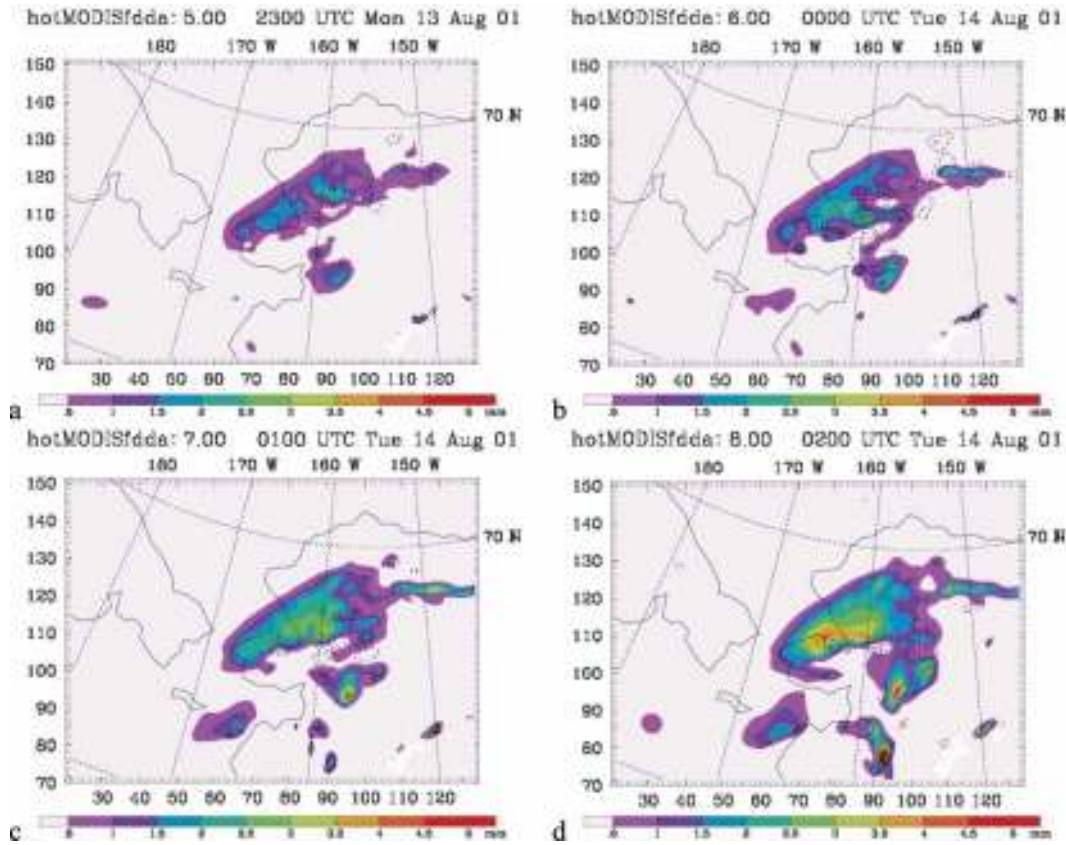


FIG. 16. Same as in Fig. 15, but for experiment hotMODISfdda for forecast hours 5–8 (2300 UTC 13 Aug–0200 UTC 14 Aug 2001). Contours show the precipitation difference (mm), hotMODISfdda – Ctrlfdda.

data adds mesoscale information and improves both the positions and spacing of the various rainfall maxima.

Another way of verifying a precipitation forecast is through use of the equitable threat score (ETS) and bias statistics, both of which are based on a contingency table approach (Wilks 1995; Colle et al. 1999). The contingency table is shown in Table 3. It is a 2×2 matrix, where each element of the matrix holds the number of occurrences in which the model and the observations did or did not reach a certain threshold amount of accumulated precipitation. Based on the contingency table, a bias score is defined as

$$\text{Bias} = \frac{F}{O} = \frac{A + B}{A + C}, \quad (6)$$

where F is the number of forecasts at the observation stations with precipitation equal or exceeding a given threshold, and O is the number of occurrences in which the observations meet or exceed the threshold. Thus, the bias score indicates how well the model predicts the frequency of occurrence of a given threshold, although it provides no information on the accuracy of forecasts.

The bias of a perfect forecast equals 1. The ETS measures the skill in predicting a given threshold at a given location and is defined by

$$\text{ETS} = \frac{H - E}{F + O - H - E} = \frac{A - E}{A + B + C - E}. \quad (7)$$

Here H is the number of forecast “hits,” a hit being defined as an occurrence of both the simulated and observed precipitation meeting or exceeding a given precipitation threshold at a point. In (7), F and O are defined as above for Eq. (6), and E is defined as

TABLE 3. Contingency table for ETS and bias skill score metrics. The letters A , B , C , and D represent the number of occurrences for which the model forecast precipitation or the observed precipitations did (Yes) or did not (No) reach/exceed a given threshold value.

For a given threshold		Observation	
		Yes	No
Model	Yes	A	B
	No	C	D

$$E = \frac{FO}{N} = \frac{(A + B)(A + C)}{N}, \quad (8)$$

where N is the total number of observations utilized in the verification process (Mesinger 1996).

Both the bias and ETS scores defined in (6) and (7) only measure model accuracy based on the frequency of occurrence at or above a threshold, and thus do not measure the magnitude of the precipitation forecast error. To examine the error magnitudes, the domain-averaged absolute root-mean-square errors (rmse) between the forecast (X_i) and observed (X_i^o) precipitation are calculated by

$$\text{RMSE} = \sqrt{\frac{1}{N} \sum_{i=1}^N (X_i - X_i^o)^2}. \quad (9)$$

For the Ctrl, hotMODIS, Ctrlfdda, and hotMODIS-fdda experiments, the ETS and bias scores are calculated using the definitions (6)–(8), for 6-h accumulated rainfall at the thresholds 0.2, 1.0, 2.5, 5.0, and 8.0 mm. Because gridded rainfall observations may introduce noise as a result of the gridding process (e.g., see Fig. 3), the ETS and bias scores are computed using only station observations of precipitation. Accordingly, the model forecast of the closest grid point to a station is used in this study as the model forecast for the station. The results are shown in Fig. 17.

During the first 6-h assimilation period, MODIS data almost had no impact, except a slight increase of ETS for the 1.0-mm threshold. The use of nudging, with or without MODIS data, also adds little or no value to the ETS and bias. The reason is that, during this period, the model state is undergoing large changes from the ingestion of MODIS data and/or the nudging constraints (at least for the given nudging coefficients), and therefore, the comparison is not well posed during this period because of the adjustment process.

During the 6–12-h forecast period, which corresponds to the first 6-h free forecast period, the use of MODIS data alone in the assimilation process leads to slightly greater skill in forecasting the larger threshold amounts (2.5, 5.0, and 8.0 mm). When MODIS information is used together with the Newtonian nudging, greater skill results at all precipitation thresholds, and the bias score approaches the perfect forecast value of 1.0.

In the second 6-h free forecast period (i.e., the 12–18-h forecast period), there appears to be a continuation of the improvement in precipitation forecast skill associated with the assimilation of MODIS-retrieved humidity in the simulation, particularly for the larger thresholds. However, precipitation skill is not, in gen-

eral, as high as for the previous 6-h period. The potential impact of MODIS-retrieved humidity information appears, at least on a domain-averaged basis, to decrease with increasing forecast length (see 24 h in Fig. 17), which is not necessarily surprising since other influences (upstream systems propagating into the model domain) play progressively larger roles in the precipitation forecast with time.

For the free forecast periods of 6–24 h in Fig. 17, a Student's t test has been performed to investigate the statistical significance of the MODIS data assimilation. The ETS and bias scores from both hotMODIS and hotMODISfdda are tested against those scores from Ctrl and CtrlFdda, including all the rainfall thresholds. The test result shows a significant improvement of the ETS score at the 95% ($\alpha < 0.05$) confidence level, and the absolute value of (bias – 1.0) is significantly reduced, which means the bias scores approaching to the perfect forecast value of 1.0, at the 85% confidence level.

As noted above, in order to determine if there are systematic errors in the magnitude of the precipitation forecast, other statistics such as the rmse are needed. Figure 18 illustrates rmse for the various experiments calculated against the station observations, using (9). Clearly, the experiments utilizing MODIS data, with or without nudging, are associated with lower rmse during the free forecast period, most notably at the 12- and 18-h forecast times. The Student's t test on the rmse for the total 18-h free forecast period indicates that MODIS data assimilation improved the forecast of precipitation magnitude, at the 80% confidence level. Taken together with the previous results, it could be argued that the assimilation of MODIS humidity improves not only the frequency, but also the magnitude of the model precipitation forecast.

d. Other atmospheric state variables

Previous studies (e.g., Harms et al. 1992; Kalnay 2003) have often shown that while inclusion of particular observations or data assimilation techniques improves the forecast skill for a particular variable of interest, the forecast skill for other variables is either unchanged or degraded. As such, it is important to determine if the use of MODIS data and the hot start techniques have favorable or negative impacts on the forecast of other atmospheric variables. Therefore, in this subsection we examine this issue in the context of atmospheric state variables at the surface level. The greater sample size of surface observations (about 500 instead of upper-air observations (less than 25 in the domain) assures for statistically confident results. The variables considered are 2-m temperature (T2), 2-m

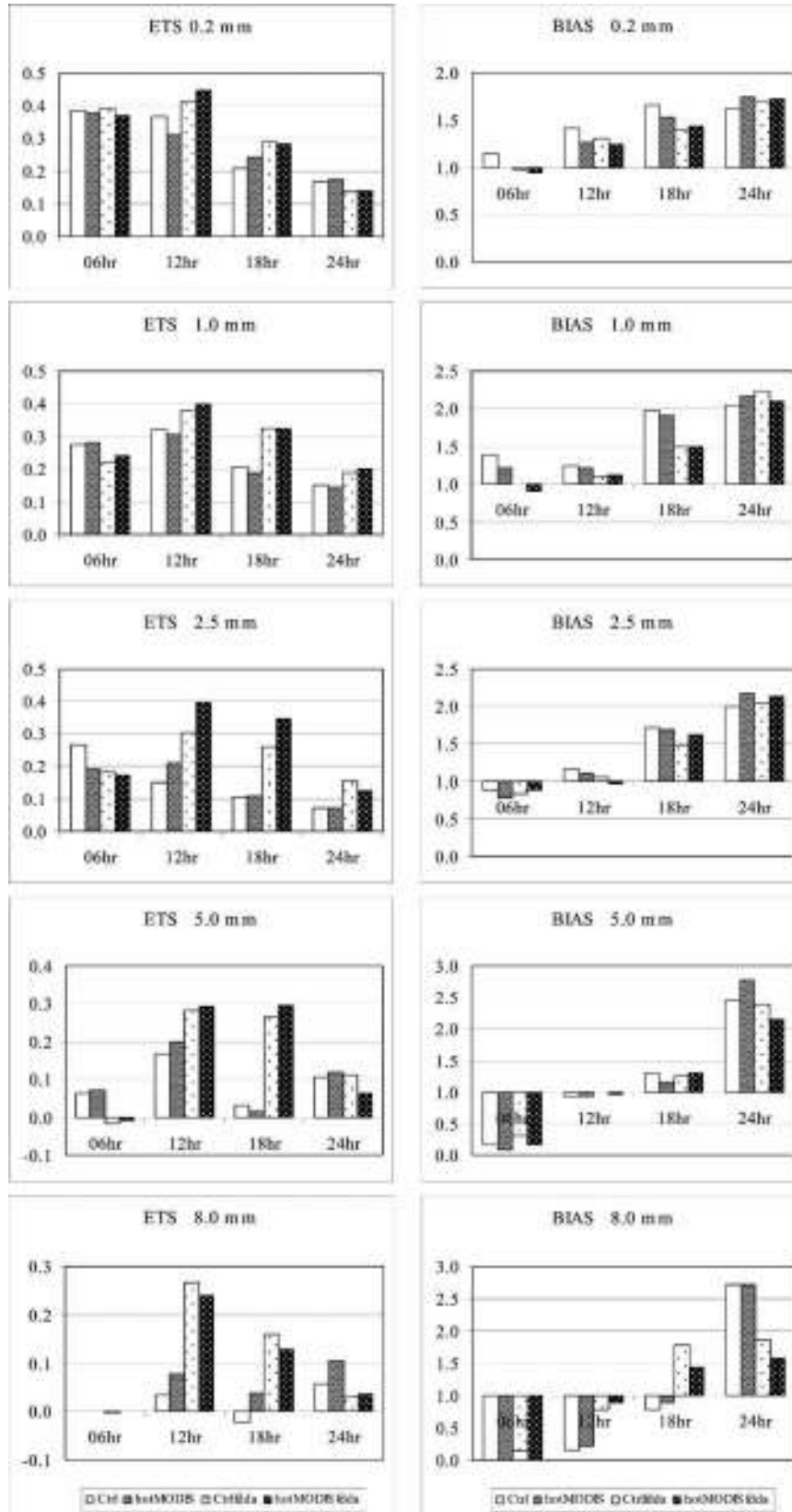


FIG. 17. (left) ETS and (right) bias score of MM5 forecasts of 6-h accumulated precipitation against station observations for the thresholds (top to bottom) 0.2, 1.0, 2.5, 5.0, and 8.0 mm.

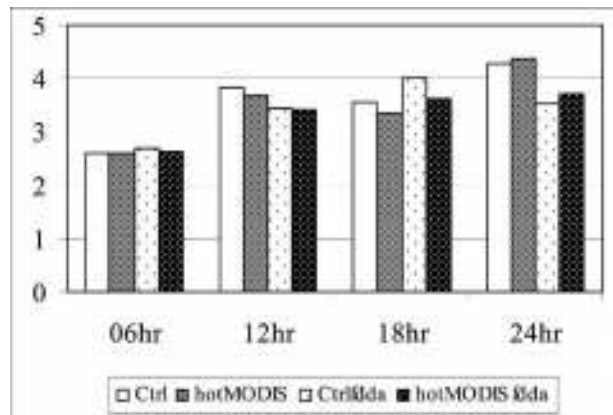


FIG. 18. Domain-averaged RMSE, for experiments Ctrl, hotMODIS, Ctrlfdda, and hotMODISfdda of 6-h accumulated precipitation forecasts verified against station observations. Key provided in figure.

relative humidity (RH2), 10-m zonal and meridional winds (U10, V10), and sea level pressure (SLP). The rmse is calculated between the model forecast and the surface observations using (9). Another statistic calculated is the mean bias (MB) of the forecasts (X_i) compared to the observations (X_i^o), defined by (N denotes the number of observations):

$$MB = \frac{1}{N} \sum_{i=1}^N (X_i - X_i^o). \quad (10)$$

Figure 19 shows domain-averaged rmse and MB statistics. During the first 6-h (i.e., the “preforecast”) period, the assimilation of MODIS data are associated with an increase of rmse in the RH2 field, which is an acceptable result, since the model state variables are undergoing adjustment processes while assimilation of data occurs during this period. Although the assimilation has led to an increased rmse in the preforecast period, the rmse in the 6–18-h free forecast period (Fig. 19) is generally reduced in the experiments with MODIS data assimilated, consistent with the results in previous sections. Specifically, the rmse in RH2 during the first two 6-h free forecast periods (forecast hours 12 and 18) is reduced, as are the positive mean biases of RH2 during these two periods. The t -test results indicate that the experiments with MODIS data assimilated significantly, at the confidence level of 99%, improved the rmse metric in this period. After 12 h of free forecast (see the 24-h period in Fig. 19), the rmse and MB scores increased in RH2 for experiments with MODIS data assimilated. Again, this is most likely due to the fact that the impact of the MODIS information ingested in the preforecast period has faded out while other influences (e.g., the boundary conditions) are more significant.

The surface temperature field does not show significant changes in rmse; however, the MB has been significantly reduced at the 95% confidence level. This reduced cold bias relates to the improved wind fields from assimilating the MODIS data, indicated by rmse and MB metrics. During the entire free forecast period, the rmse of the zonal and meridional winds are less in the experiments utilizing MODIS data. Moreover, the MODIS data assimilation also appears to be associated with reduced positive mean biases. The t tests on U and V also indicate that the improvements in rmse are significant at the 95% and 99% confidence levels, and that the improvements in MB are significant at the 85% and 97% confidence levels, respectively. The reduced positive mean biases indicates that the two simulations utilizing MODIS data partially correct the tendency for the propagation of the precipitation systems to be too rapid (eastward and northward) in experiments Ctrl and hotMODIS. The use of Newtonian nudging (e.g., experiment hotMODISfdda) provides even further improvement in this regard. However, the nudging experiments Ctrlfdda and hotMODISfdda caused a degree of degradation in the 24-h wind forecast. The reason may be that only the gridded analysis nudging is used in this study so the model relaxes to the analyzed field during integration. Errors of the gridded analysis might have been carried into the model results. One way to overcome this problem is to apply observation nudging in tandem with the analysis nudging so that the model evolution is also constrained by station observations.

By contrast, the assimilation of MODIS humidity has little impact on surface temperature and sea level pressure fields; the surface temperature result, however, suggests that there is little adverse impact to the simulated surface sensible and latent heat flux exchanges via the introduction of MODIS data, an important consideration. It would not be desirable for a humidity adjustment to change the surface flux balance, which would occur if serious impacts to the temperature were noted.

Another phenomenon shown in Fig. 19’s temperature and relative humidity fields is the likely diurnal trend that is associated with the local synoptic environment. As discussed by Mass et al. (2002), the diurnal trend exists in the MM5 forecast skills even when higher horizontal resolution is applied.

Now, consider Fig. 1. In the cloudy area, CtrlC0 has large errors in precipitable water and precipitation mass and needs at least 1 h to adjust, while hotMODC0 catches valuable information from satellite data and MM5 forecast. In addition, in the clear area, while the continuous run ContC-6 maintains more precipitation mass, the hotMODC0 run gets information from the

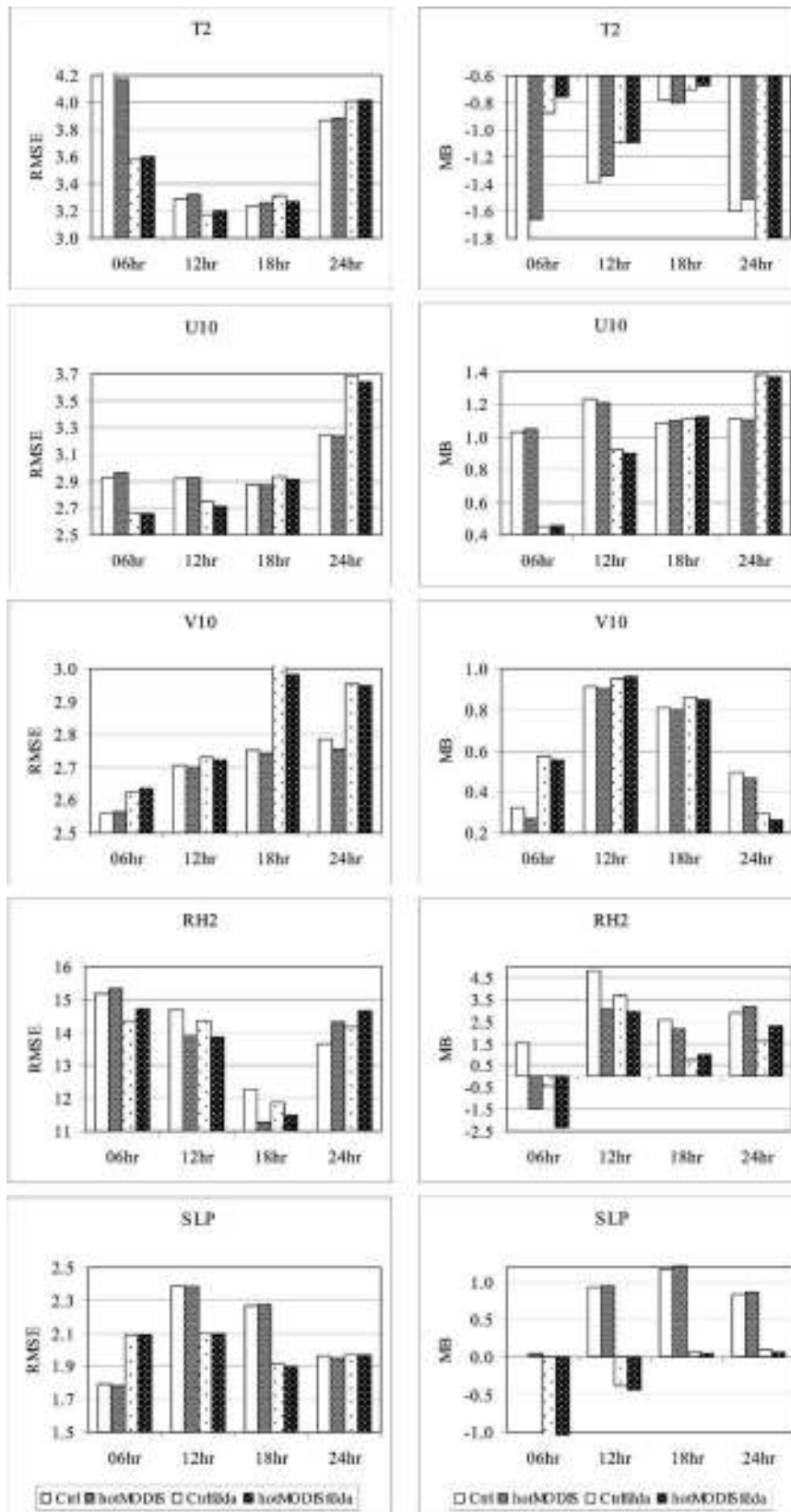


FIG. 19. Domain-averaged (left) RMSE and (right) MB for experiments Ctrl, hotMODIS, Ctrlfdda, and hotMODISfdda of forecasted (top to bottom) surface 2-m temperature (T2), 10-m winds (U10, V10), 2-m relative humidity (RH2), and SLP. Key provided in figure.

satellite and goes with CtrlC0. Experiment CtrlC0 produces false cloud water and ice, which is not produced in hotMODC0.

5. Extensive tests and results

The results of assimilating MODIS-retrieved cloud and humidity profiles in the preliminary test case are promising. However, in order to obtain a general conclusion about the proposed method and the MODIS data assimilation, further extensive testing is necessary. An additional 16 simulation tests focusing on two 3-day periods, one in winter and one in summer, have been conducted. The results of these tests are presented in this section.

a. Description of test cases

Winter and summer are the two major seasons at high latitudes, so the extensive test cases are selected from both seasons. The 3-day period of 19–22 July 2002 is chosen for summer, while the 10–13 February 2003 period is chosen for winter. Similar to the preliminary test case, each case will consist of a 24-h forecast simulation. However, the preforecast period in these cases consists of the first 12 h, to allow for more satellite data to be ingested. As a result, during the preforecast period, the model should be influenced by more realistic cloud and humidity distributions and theoretically be constrained closer to the real atmosphere. Further, the utility of the simulation for diagnostic purposes during the data-ingest period can be investigated. Due to the high degree of nonlinearity of atmospheric models, small perturbations of initial conditions can produce large differences on forecasts (e.g., Crook 1996; Martin and Xue 2004). In addition, a model that is initialized at different times could also result in different forecast solutions (Bua 2003). To diversify the numerical experiments, eight separate 24-h simulations from each 3-day period, each initializing 6 h apart, are conducted. For the winter cases, the initial times are 0600, 1200, and 1800 UTC 10 February 2003; 0000, 0600, 1200, and 1800 UTC 11 February 2003; and 0000 UTC 12 February 2003. For the summer cases, the initial times are 0600, 1200, and 1800 UTC 19 July 2002; 0000, 0600, 1200, and 1800 UTC 20 July 2002; and 0000 UTC 21 July 2002. Four experiments (Ctrl, hotMODIS, Ctrlfdda, and hotMODISfdda as defined in Table 2) have been performed for each initial time.

b. Results

For obtaining a general conclusion about the method and data, we focus here on the impacts of the MODIS

data assimilation, using the hot start technique, on the forecast of model state variables and precipitation.

For these 16 cases, the model results are verified against both the MM5 analyses and station observations. Verification against the analyses, particularly for the state variables, is useful in determining the impacts of the MODIS data assimilation on the larger meteorological scales, while verification against the observations provides information on the impacts relative to smaller-scale precipitation processes. For the verification against the MM5 analysis, the rmse and MB scores have also been computed for the three-dimensional temperature (T), wind (U , V , W), water vapor mixing ratio (Q), and pressure perturbation (PP) fields, as well as for the two-dimensional SLP field.

For ease of comparison, and to clearly show the differences between experiments, a skill score (SS) based on the rmse is defined following Wilks (1995) as

$$\begin{aligned} SS &= \left(\frac{\text{RMSE} - \text{RMSE}_{\text{ctrl}}}{0 - \text{RMSE}_{\text{ctrl}}} \right) 100\% \\ &= \left(1 - \frac{\text{RMSE}}{\text{RMSE}_{\text{ctrl}}} \right) 100\%, \end{aligned} \quad (11)$$

where $\text{RMSE}_{\text{ctrl}}$ is the rmse between the control experiment and the analysis for verification against the MM5 analysis; RMSE is the corresponding rmse between the particular experiment in question (excluding the Control) and the analysis. According to this definition, the skill score SS is interpreted as a percentage improvement of the particular experiment in question over the control forecasts for the variable of interest.

The SS metrics that are computed compare the following: 1) the hotMODIS experiment to the Ctrl experiment, and 2) the hotMODISfdda experiment to the Ctrlfdda experiment. These metrics can be used to study the impacts of MODIS assimilation using the hot start approach. Since there are 16 simulation study periods (8 for the July 2002 case, 8 for the February 2003 case), 32 SS metrics, providing information on the benefit of the use of the MODIS hot start technique, result for each variable. In Table 4 we present the average values of the SS metric across these cases, stratified into the values for the winter and summer cases, respectively. Due to the nature of the assimilation approach in which the model humidity field is adjusted according to satellite retrievals, there are large negative skill scores for the water vapor mixing ratio Q for both winter and summer cases. These negative skill scores indicate the percentage that Q has been changed during the humidity adjustment stage and the effect of this change on later times. This is expected to happen when verifying

TABLE 4. Domain and case-averaged SS metric (%) indicating the relative improvement (positive values) or degradation (negative values) of forecasts from experiments hotMODIS and hotMODISfdda over forecasts from experiments Ctrl and Ctrlfdda, respectively, verified against the MM5 analyses.

	Winter				Summer				
	6 h	12 h	18 h	24 h	6 h	12 h	18 h	24 h	
<i>T</i>	0.80	1.28	0.64	0.64	<i>T</i>	0.40	1.80	3.62	4.10
<i>U</i>	-0.25	-0.20	0.17	0.33	<i>U</i>	0.07	0.21	0.71	0.76
<i>V</i>	0.01	-0.01	-0.04	-0.31	<i>V</i>	-0.01	-0.06	0.64	0.48
<i>W</i>	-0.57	-0.19	0.68	0.23	<i>W</i>	0.32	0.93	2.54	1.03
<i>Q</i>	-32.28	-31.86	-15.99	-7.66	<i>Q</i>	-32.99	-27.42	-14.69	-9.65
PP	0.03	0.01	-0.15	-0.45	PP	0.28	0.72	0.84	1.45
SLP	-0.02	0.34	0.76	0.83	SLP	0.28	1.58	2.46	3.50

against the MM5 analysis that is providing the Ctrl experiment initial and boundary conditions. Meanwhile, according to the definition (11), the SS scores are calculated with reference to the rmse of a control experiment. Thus, the large negative SS values for *Q* of a hotMODIS experiment actually imply the difference between the MM5 analysis and the MODIS retrieved values (i.e., how much of the MM5-analyzed *Q* has been adjusted by assimilating the MODIS data). Also as we can see from Table 4, the magnitudes of those large negative SS values shown for the preforecast periods' *Q* decrease gradually with time during free forecast periods, consistent with the fact that no additional humidity adjustment is occurring via the hot start process.

The skill scores show that, on a gross average scale (3D column and domain averages), the free forecasts of *T*, *U*, *W*, and SLP are slightly improved for the winter cases with the use of MODIS data in a hot start mode. By contrast, the forecasts of *V* and PP are degraded. However, for the summer cases, the forecast of all variables except the water vapor mixing ratio *Q* are improved through the assimilation of MODIS data. Because the mixing ratio *Q* is the variable we adjust in the hot start process, as mentioned above, verification against the MM5 analysis only indicates at what extent (percentage) that *Q* is modified. Its forecast skill can only be verified against station observations.

Table 5 lists the skill scores for the surface variables

T2, U10, V10, RH2, and SLP verified using surface station observations. To summarize, significant degradation is evident with the use of a MODIS hot start approach in the winter case, while significant improvement is apparent (as evidenced by large positive SS values) in most surface variables across the forecast period for the summer case. The degradation for the winter case raises questions for future study related to satellite data assimilation. First, the winter atmospheric environment at high latitudes is very different from summertime. For example, due to the extremely cold temperatures, less water clouds but more ice clouds are present at lower levels. Therefore, for this study, the relative humidity thresholds derived from a summer case may not be suitable for this case or other winter cases. Other possible factors related to the poor performance include snow cover and sea ice that may affect the MODIS data quality, and poor simulation of complex boundary layer structures, which in turn affect the surface simulation, and correspondingly, the verification results.

For the precipitation verification, ETS and bias are calculated for each case. Average ETS and bias scores are shown in Fig. 20 for the summer cases and in Fig. 21 for the winter cases. For summer precipitation, Fig. 20 shows that the assimilation of MODIS data has significantly improved the skills in simulating the precipitation frequencies during the assimilation (0–12 h) period; the 99% confidence level is satisfied in a *t* test.

TABLE 5. Same as in Table 4, but verified against station observations of surface variables.

	Winter				Summer				
	6 h	12 h	18 h	24 h	6 h	12 h	18 h	24 h	
T2	-0.18	-1.47	-1.29	-0.60	T2	1.34	3.96	3.39	3.43
U10	-0.54	-0.94	-0.66	0.07	U10	-0.47	-0.20	0.44	1.70
V10	-0.24	-0.55	-0.05	0.91	V10	-0.26	0.62	1.60	0.90
RH2	1.57	1.08	-0.66	-0.07	RH2	11.10	16.83	12.66	8.51
SLP	-0.21	-0.01	0.55	-1.12	SLP	-0.38	0.43	3.03	4.33

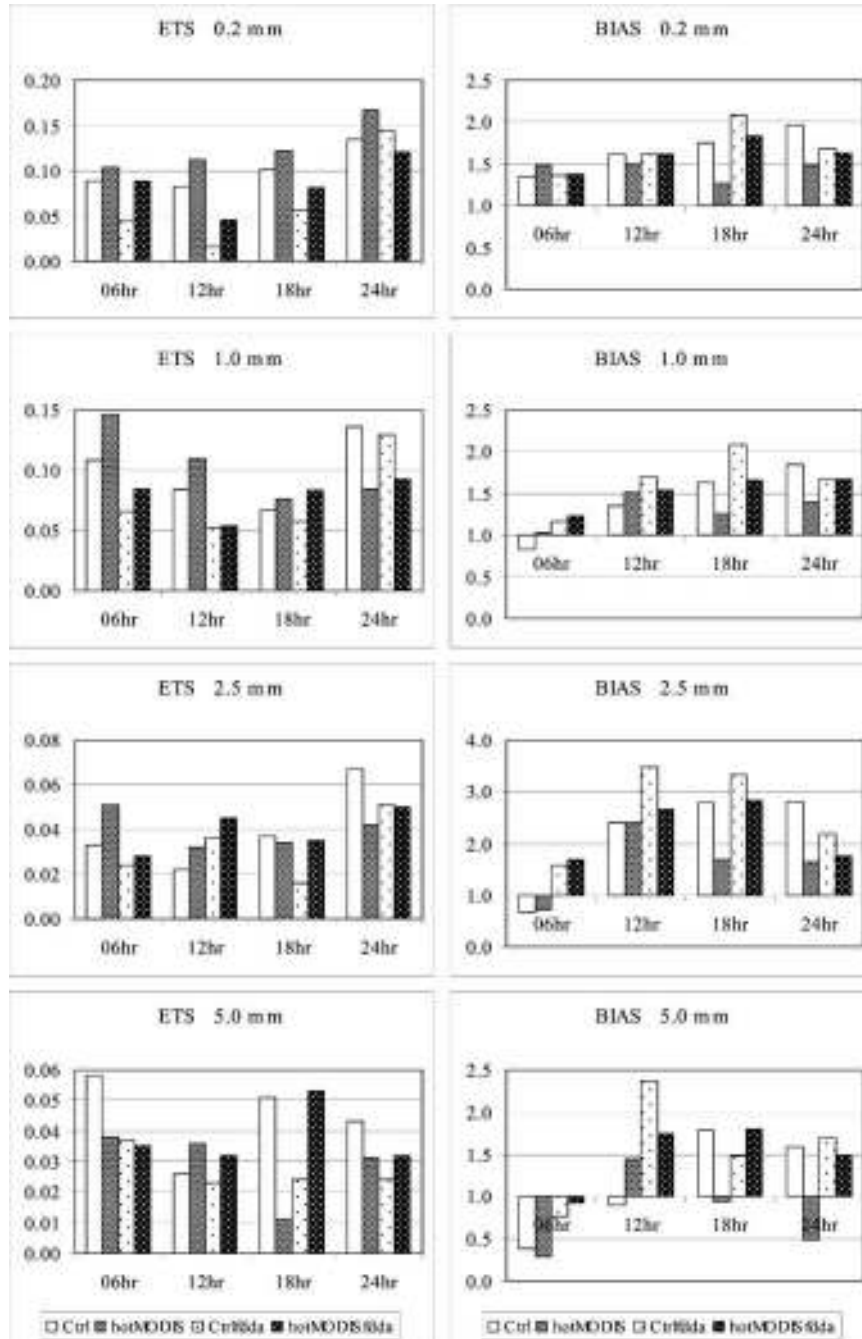


FIG. 20. (left) ETS and (right) bias scores averaged over the domain for the 16 summer case experiment hotMODIS and hotMODISfdda realizations, pertaining to 6-h forecasts of accumulated precipitation verified against station observations for the thresholds (top to bottom) 0.2, 1.0, 2.5, and 5.0 mm.

During the first 6-h free forecast (forecast hour 18) periods, the precipitation forecast skill (ETS) is improved at the 90% confidence level for all the four precipitation thresholds within the experiments that the MODIS data are assimilated. No significant improve-

ment is shown for the 12-h free forecast (forecast error 24) ETS scores. The relative benefit of the MODIS data at the 24-h forecast time is less, as the external boundary conditions from the start of the forecast (and their inherent errors) now influence a significant part of the

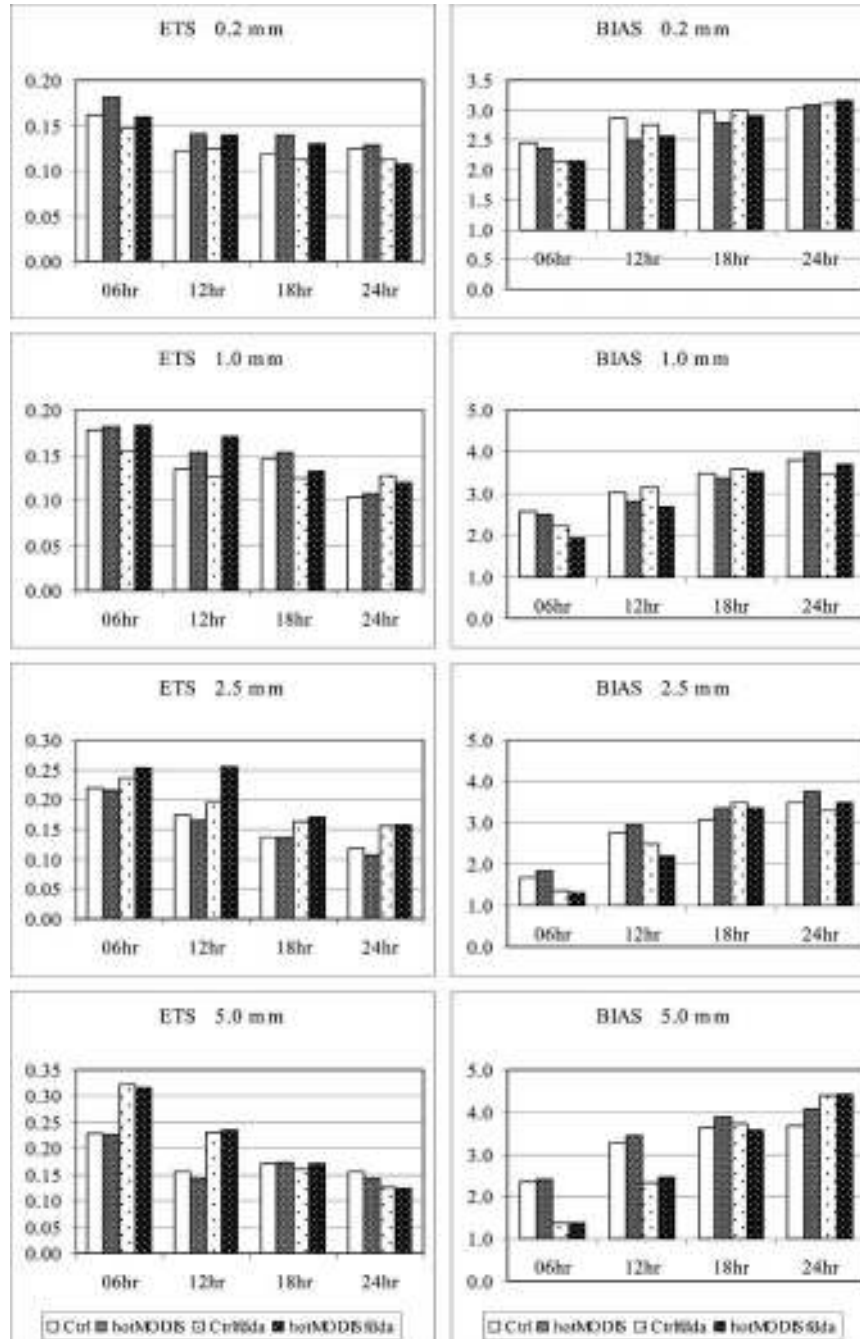


FIG. 21. Same as in Fig. 20, but for the 16 winter case experiment hotMODIS and hotMODISfdda realizations.

domain. However, the bias scores' t test shows significant improvement at the 99% confidence level for both 6-h free forecast periods.

For the winter cases (Fig. 21), application of MODIS data provides a significant improvement on simulation skills indicated by the ETS score, which is at the 99% confidence level in the t test. For the first 6-h free forecast period, ETS scores have benefited from the

MODIS data assimilation; confidence level of 97% is shown in the t test. However, the second 6-h free forecast did not benefit from the MODIS data assimilation.

6. Summary and conclusions

This paper describes research in which a "hot start" technique was developed for the MM5 model to dy-

namically assimilate MODIS-retrieved cloud properties and humidity profiles. This hot start assimilation approach has been studied for high-latitude rain events. In addition to a detailed study and analysis for a preliminary test case, the results of extensive experiments have been presented in order to support more general conclusions as to the benefit of this technique. The feasibility of both the assimilation approach and the benefit to the simulated/forecast fields has been demonstrated.

Ingestion of real-time MODIS-retrieved cloud and clear-air humidity information results in commensurate adjustments to the MM5 humidity field. The MODIS data ingestion impacts the MM5 cloud fields from both a microphysical and a macrophysical standpoint. Microphysically, the humidity adjustments impact the cloud hydrometeor fields. Macrophysically, the adjustments are manifested in the horizontal cloud coverage distribution and the cloud-top temperature.

The impact of the MODIS hot start scheme on short-term (6–12 h) forecasts of precipitation and other atmospheric variables has been the key focus of this paper. The primary conclusions of the present research are as follows:

- It is feasible to introduce MODIS-retrieved cloud-top properties and humidity profile information into the MM5 model through a hot start humidity adjustment procedure that does not disrupt either model stability or evolutionary continuity.
- The introduction of high-resolution MODIS information produced more accurate relative humidity forecasts through modification to the model water mixing ratio field, which further resulted in increased meso-scale structure in the cloud hydrometeor and precipitation fields.
- The opportunistic ingestion of MODIS data at its observation time into the model provides temporally accurate information, leading to significantly improved 6-h model precipitation forecasts on not only the frequency of occurrences, but also the magnitude of precipitation amounts for all the summer and winter cases. Some improvement has also been shown on 12-h precipitation forecasts.
- Verification against three-dimensional analyses indicates that the model forecasts of temperature, wind, pressure perturbation, and sea level pressure are all improved for the summer cases, as indicated by an average 2% increase in forecast skill over all atmospheric state variables over all summer cases. A slight improvement for the winter cases is shown by a 0.5% increase in forecast skill averaged over all atmospheric-state variables over all winter cases.
- Verification against surface station observations indicates that the model forecasts of 2-m temperature, 2-m relative humidity, 10-m winds, and sea level pressure are all improved for the summer cases, as indicated by a 4% improvement in forecast skill averaged over all surface variables and all summer cases. The largest improvement in forecast skill is for 2-m relative humidity (12%). There is significant degradation in forecast skill for the winter cases.

The above points suggest that the ingestion and assimilation of MODIS data provides added value to not only on precipitation forecasts from the MM5 modeling system, but also for forecasts of other atmospheric variables. However, the improvement for the winter cases was substantially less than for the summer cases. One possible reason for this disparity is that the relative humidity thresholds used for determining the humidity adjustment were empirically derived to apply primarily to warm season conditions (Fan and Tilley 2002). Thus, the seasonal variation of clouds and humidity at high latitude should be taken into account for future applications of the method, especially for the winter season.

In agreement with previous studies, the comparison between experiments utilizing the standard MM5 Newtonian nudging technique with the experiments that did not suggested (e.g., Fan and Tilley 2001) that NWP forecasts in high latitudes can benefit from the nudging technique. Further, a comparison of two experiments—hotMODIS and hotMODISfdda—that combined the two data assimilation methodologies indicates that forecast skill is further improved by the joint application of the two methodologies. This result implies that other products derived through satellite retrieval techniques could be assimilated via the hot start approach introduced here, Newtonian nudging, or even a variationally based scheme such as 3DVAR, and lead to a continued improvement in model forecast skill for high-latitude applications. For example, cloud drift and water vapor drift wind fields (Key et al. 2003) could be ingested to help maintain the proper advective forcing for the cloud fields, and subsequently lead to improved forecasts. Other possibilities are the precipitable water and wind retrievals from the NASA/NOAA Television Infrared Observation Satellite (TIROS) Operational Vertical Sounder (TOVS) polar pathfinder, which provides high-resolution complementary data to the sparse rawinsonde observation network in the polar regions (Francis 2002; Groves and Francis 2002). Combined utilization of all these data sources would be valuable for future studies of weather and climate in the polar regions, especially for an Arctic regional reanalysis program. Such a reanalysis program would provide dy-

namically consistent fields that are sparse or problematic in direct observations (e.g., precipitation, evapotranspiration, radiation, and clouds) at higher spatial and temporal resolution, and with greater reliability, than from current reanalyses (Serreze et al. 2003; Hines et al. 2000).

While the ability of the MODIS hot start approach has been demonstrated throughout this paper to have a positive influence on the moisture and cloud fields, correcting areas that are either too dry or too moist in the model simulation, there are still ways in which the scheme can be improved and optimized. One of these ways is related to the fact that when water mass is changed at the grid point (via adjustment of the water vapor mixing ratio according to relative humidity profiles determined), there is the potential for horizontal diffusion within the model [formulated using a fourth-order scheme, see Grell et al. (1994)] to interact with the adjustment process and affect the desired formation or dissipation of cloud.

An example of such an occurrence is illustrated in Fig. 22, which focuses on a grid point near the lower Yukon Valley (cf. Fig. 3d), in the mid- to upper troposphere (sigma level 20). This grid point is indicated cloudy at 0000 UTC 14 August 2001 by the MODIS observation; and the water vapor mixing ratio has been adjusted from sigma level 18 to 37 in experiment hotMODIS. Shown in the figure are, for the Ctrl and hotMODIS experiments, respectively, the contribution to the water vapor mixing ratio tendencies from horizontal diffusion as well as the evolution of the water vapor mixing ratio and relative humidity for 1 h after the MODIS data insertion time (at 360 min into the forecast simulation). In addition to a minor initial gravity wave-type oscillation (which appears in virtually all fields due to the addition of water mass) in experiment hotMODIS, Fig. 22a indicates that a significant negative tendency in the water vapor mixing ratio due to diffusion within the first few minutes after insertion. The diffusive tendency, though on a relatively longer time scale compared with the gravity wave oscillation, still becomes less pronounced with time and is minimal approximately 22 min after the adjustment occurs. Though neither the gravity wave nor diffusion effects are very desirable, they do not negate the overall benefit of the adjustment, as illustrated by the actual values and evolution of vapor mixing ratio during the same period in Fig. 22b. The adjustment process in the hotMODIS experiment results in a nearly 30% increase of the water vapor mixing ratio, which is followed by a 10% loss during the period that the diffusion effect is significant. The 10% loss still allows for the modified

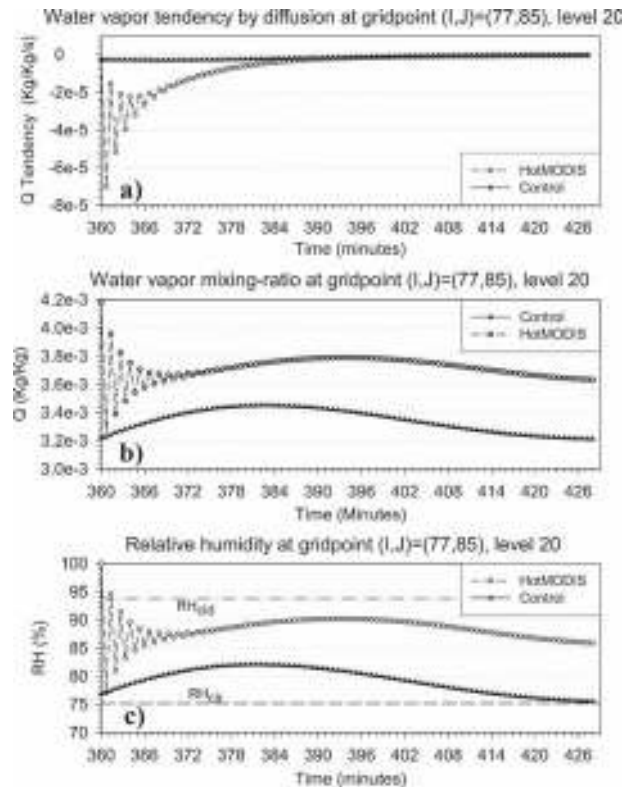


FIG. 22. (a) Tendencies for the water vapor mixing ratio Q ($\text{kg kg}^{-1} \text{s}^{-1}$) due to diffusion in the Ctrl and hotMODIS experiments, for grid point $(I, J) = (77, 85)$ at sigma level 20; (b), (c) evolutions in Q (kg kg^{-1}) and relative humidity (RH, %), respectively, during the same period, at the same point and vertical level, for experiments Ctrl and hotMODIS. The RH thresholds RH_{cl} and RH_{cr} for level 20 are shown in (c) with dash-dotted and dashed lines, respectively. The insertion of MODIS data occurs at 360 min into the forecast simulation in experiment hotMODIS; and the plots indicate the time period of 360–428 min.

water vapor mixing ratio (and by extension the relative humidity) to be much higher than is the case in the Ctrl simulation, and the relative humidity values (Fig. 22c) never drop below the critical value of RH_{cr} ; as such the cloud that would form in this case remains intact, though some redistribution of water mass to adjacent points has likely occurred via diffusion.

The example in Fig. 22 is a relatively extreme one in that it considers a grid point where a water vapor mixing ratio adjustment is made with MODIS data in isolation from its neighbors. In many instances, adjustments occur for a cluster of neighboring points, thus the diffusion effect would be expected to be less than depicted in Fig. 22. Nonetheless, this effect does lead to a slightly suboptimal utilization of the moisture information, and in future work we intend to develop an appropriate method to mitigate this effect without introducing other artificialities into the model evolution.

Acknowledgments. The study is supported by the University Partnering for Operational Support (UPOS) Program of the Department of Defense, administered by Johns Hopkins University. Thanks to the two anonymous reviewers for the constructive suggestions and comments. Thanks to Xiande Meng and Jeremy Krieger for data assistance; and to the UAF GINA facility and Kevin Engle for MODIS assistance. The data used in this study were acquired as part of the NASA's Earth Science Enterprise. The algorithms were developed by the MODIS Science Teams and the data were processed by the MODIS Adaptive Processing System (MODAPS) and Goddard Distributed Active Archive Center (DAAC), and are archived and distributed by the Goddard DAAC.

REFERENCES

- Bayler, G. M., R. M. Aune, and W. H. Ramond, 2000: NWP cloud initialization using GOES sounder data and improved modeling of nonprecipitating clouds. *Mon. Wea. Rev.*, **128**, 3911–3920.
- Bua, B., 2003: Short-range ensemble forecasts and initial conditions: The 6–7 January 2002 Northeast snowstorm. *Bull. Amer. Meteor. Soc.*, **84**, 562–566.
- Chen, F., and J. Dudhia, 2001: Coupling an advanced land surface hydrology model with the Penn State/NCAR MM5 modeling system. Part I: Model description and implementation. *Mon. Wea. Rev.*, **129**, 569–585.
- Colle, B. A., K. J. Westrick, and C. F. Mass, 1999: Evaluation of MM5 and Eta-10 precipitation forecasts over the Pacific Northwest during the cool season. *Wea. Forecasting*, **14**, 137–154.
- Cressman, G. P., 1959: An operational objective analysis system. *Mon. Wea. Rev.*, **87**, 367–374.
- Crook, N. A., 1996: Sensitivity of moist convection forced by boundary layer processes to low-level thermodynamic fields. *Mon. Wea. Rev.*, **124**, 1767–1785.
- Dudhia, J., 1989: Numerical study of convection observed during the winter monsoon experiment using a mesoscale two-dimensional model. *J. Atmos. Sci.*, **46**, 3077–3107.
- , D. O. Gill, K. Manning, W. Wang, and C. Bruyere, 2005: PSU–NCAR MM5 Tutorial Class Notes and User's Guide: MM5 Modeling System Version 3. 266 pp + appendixes. [Available online at http://www.mmm.ucar.edu/mm5/documents/MM5_tut_Web_notes/tutorialTOC.htm.]
- Fan, X., and J. S. Tilley, 2001: Application of the Bratseth scheme for high latitude intermittent data assimilation using the PSU/NCAR MM5 mesoscale model. Preprints, *18th Conf. on Weather Analysis and Forecasting/14th Conf. on Numerical Weather Prediction*, Ft. Lauderdale, FL, Amer. Meteor. Soc., CD-ROM, JP1.11.
- , and —, 2002: The impact of assimilating AVHRR-derived humidity on high-latitude MM5 forecasts. Preprints, *15th Conf. on Numerical Weather Prediction*, San Antonio, TX, Amer. Meteor. Soc., CD-ROM, P1.4.
- , and —, 2003: Tests of a satellite-based cloud initialization scheme for high-latitude application in MM5. Preprints, *Seventh Conf. on Polar Meteorology and Oceanography*, Hyanis, MA, Amer. Meteor. Soc., CD-ROM, 9.6.
- Francis, J. A., 2002: Validation of reanalysis upper-level winds in the Arctic with independent rawinsonde data. *Geophys. Res. Lett.*, **29**, 1315, doi:10.1029/2001GL014578.
- Garand, L., and S. Nadon, 1998: High-resolution satellite analysis and model evaluation of clouds and radiation over the Mackenzie Basin using AVHRR data. *J. Climate*, **11**, 1976–1996.
- Grell, G. A., 1993: Prognostic evaluation of assumptions used by cumulus parameterizations. *Mon. Wea. Rev.*, **121**, 764–787.
- , J. Dudhia, and D. R. Stauffer, 1994: A description of the fifth-generation Penn State/NCAR mesoscale model (MM5). NCAR Tech. Note NCAR/TN-398+ST, 117 pp.
- Groves, D. G., and J. A. Francis, 2002: Moisture budget of the Arctic atmosphere from TOVS satellite data. *J. Geophys. Res.*, **107**, 4391, doi:10.1029/2001JD001191.
- Haag, W., B. Karcher, J. Strom, A. Minikin, J. Ovarlez, U. Lohmann, and A. Stohl, 2003: Freezing thresholds and cirrus cloud formation mechanisms inferred from in situ measurements of relative humidity. *Atmos. Chem. Phys.*, **3**, 1791–1806.
- Harms, D. E., S. Raman, and R. V. Madala, 1992: An examination of four-dimensional data-assimilation techniques for numerical weather prediction. *Bull. Amer. Meteor. Soc.*, **73**, 425–440.
- Hines, K. M., D. H. Bromwich, and G. J. Marshall, 2000: Artificial surface pressure trends in the NCEP–NCAR reanalysis over the Southern Ocean and Antarctica. *J. Climate*, **13**, 3940–3952.
- Hong, S. Y., and H. L. Pan, 1996: Nonlocal boundary layer vertical diffusion in a medium-range forecast model. *Mon. Wea. Rev.*, **124**, 2322–2339.
- Kalnay, E., 2003: *Atmospheric Modeling, Data Assimilation and Predictability*. Cambridge University Press, 341 pp.
- Key, J., D. Santek, C. S. Velden, N. Bormann, J.-N. Thepaut, L. P. Riishojgaard, Y. Zhu, and W. P. Menzel, 2003: Cloud-drift and water vapor winds in the polar regions from MODIS. *IEEE Trans. Geosci. Remote Sens.*, **41**, 482–492.
- King, M. D., and Coauthors, 2003: Cloud and aerosol properties, precipitable water, and profiles of temperature and humidity from MODIS. *IEEE Trans. Geosci. Remote Sens.*, **41**, 442–458.
- Lazarus, S. M., S. K. Krueger, and S. A. Frisch, 1999: An evaluation of the Xu–Randall cloud fraction parameterization using ASTEX data. Preprints, *13th Symp. on Boundary Layers and Turbulence*, Dallas, TX, Amer. Meteor. Soc., 582–585.
- Lipton, A. E., 1993: Cloud shading retrieval and assimilation in a satellite-model coupled mesoscale analysis system. *Mon. Wea. Rev.*, **121**, 3062–3081.
- , and G. D. Modica, 1999: Assimilation of visible-band satellite data for mesoscale forecasting in cloudy conditions. *Mon. Wea. Rev.*, **127**, 265–278.
- Lorenz, E. N., 1963: Deterministic nonperiodic flow. *J. Atmos. Sci.*, **20**, 130–141.
- Martin, W. J., and M. Xue, 2004: Initial convection sensitivity analysis of a mesoscale forecast using very-large ensembles. Preprints, *20th Conf. on Weather Analysis Forecasting/16th Conf. on Numerical Weather Prediction*, Seattle, WA, Amer. Meteor. Soc., CD-ROM, J8.2.
- Mass, C. F., D. Ovens, K. Westrick, and B. A. Colle, 2002: Does increasing horizontal resolution produce more skillful forecast? *Bull. Amer. Meteor. Soc.*, **83**, 407–430.
- , and Coauthors, 2003: Regional environmental prediction over the Pacific Northwest. *Bull. Amer. Meteor. Soc.*, **84**, 1353–1366.
- Menzel, W. P., B. A. Baum, K. I. Strabala, and R. A. Frey, 1997:

- Cloud top properties and cloud phase algorithm theoretical basis document. NASA GSFC, 61 pp. [Available online at http://modis-atmos.gsfc.nasa.gov/_docs/atbd_mod04.pdf.]
- , S. W. Seemann, J. Li, and L. E. Gumley, 2002: MODIS atmospheric profile retrieval algorithm theoretical basis document. NASA GSFC, 35 pp. [Available online at http://modis-atmos.gsfc.nasa.gov/_docs/atbd_mod07.pdf.]
- Mesinger, F., 1996: Improvements in quantitative precipitation forecasts with the Eta regional model at the National Centers for Environmental Prediction: The 48-km upgrade. *Bull. Amer. Meteor. Soc.*, **77**, 2637–2649.
- Peixoto, J. P., and A. H. Oort, 1992: *Physics of Climate*. American Institute of Physics, 520 pp.
- , and —, 1996: The climatology of relative humidity in the atmosphere. *J. Climate*, **9**, 3443–3463.
- Powers, J. G., A. J. Monaghan, A. M. Cayette, D. H. Bromwich, Y.-H. Kuo, and K. W. Manning, 2003: Real-time mesoscale modeling over Antarctica: The Antarctic mesoscale prediction system. *Bull. Amer. Meteor. Soc.*, **84**, 1533–1545.
- Randall, D. A., J. A. Coakley Jr., D. H. Lenschow, C. W. Fairall, and R. A. Kropfli, 1984: Outlook for research on subtropical marine stratification clouds. *Bull. Amer. Meteor. Soc.*, **65**, 1290–1301.
- Reisner, J., R. M. Rasmussen, and R. T. Bruintjes, 1998: Explicit forecasting of supercooled liquid water in winter storms using the MM5 mesoscale model. *Quart. J. Roy. Meteor. Soc.*, **124**, 1071–1107.
- Ruggiero, F. H., G. D. Modica, and A. E. Lipton, 2000: Assimilation of satellite imager data and surface observations to improve analysis of circulations forced by cloud shading contrasts. *Mon. Wea. Rev.*, **128**, 434–448.
- Serreze, M. C., M. P. Clark, and D. H. Bromwich, 2003: Monitoring precipitation over the Arctic terrestrial drainage system: Data requirements, shortcomings and applications of atmospheric reanalysis. *J. Hydrometeor.*, **4**, 387–407.
- Slingo, A., 1990: Sensitivity of the Earth's radiation budget to changes in low clouds. *Nature*, **343**, 49–51.
- Stauffer, D. R., and N. L. Seaman, 1990: Use of four-dimensional data assimilation in a limited area mesoscale model. Part I: Experiments with synoptic-scale data. *Mon. Wea. Rev.*, **118**, 1250–1277.
- Strom, J., and Coauthors, 2003: Cirrus cloud occurrence as function of ambient relative humidity: A comparison of observations obtained during the INCA experiment. *Atmos. Chem. Phys.*, **3**, 1807–1816.
- Tilley, J. S., and D. H. Bromwich, 2005: Short-to-medium range numerical weather prediction in the Arctic and Antarctic. *Bull. Amer. Meteor. Soc.*, **86**, 983–988.
- , X. Fan, and J. E. Walsh, 2005: Application of a Mesoscale 3DVAR system at high latitudes as a step towards Arctic Reanalysis. Preprints, *Eighth Conf. on Polar Meteorology and Oceanography*, San Diego, CA, Amer. Meteor. Soc., CD-ROM, JP2.11.
- Wang, J., and J. A. Curry, 1998: Relative humidity variations in the tropical western Pacific and relations with deep convective clouds. *Proc. Eighth Atmospheric Radiation Measurement (ARM) Science Team Meeting*, Tucson, AZ, ARM, 787–790.
- , W. B. Rossow, and Y.-C. Zhang, 2000: Cloud vertical structure and its variations from a 20-year global rawinsonde dataset. *J. Climate*, **13**, 3041–3056.
- Wilks, D., 1995: *Statistical Methods in the Atmospheric Sciences: An Introduction*. Academic Press, 467 pp.
- Xu, K.-M., and D. A. Randall, 1996: A semi-empirical cloudiness parameterization for use in climate models. *J. Atmos. Sci.*, **53**, 3084–3102.
- Yi, Y., P. Minnis, J. Huang, J. K. Ayers, D. R. Doelling, M. M. Khaiyer, M. L. Nordeen, 2004: Cloud detection using measured and modeled state parameters. Preprints, *13th Conf. on Satellite Oceanography and Meteorology*, Norfolk, VA, Amer. Meteor. Soc., CD-ROM, P6.11.
- Yucel, I., W. J. Shuttleworth, R. T. Pinker, L. Lu, and S. Sorooshian, 2002: Impact of ingesting satellite-derived cloud cover into the Regional Atmospheric Modeling System. *Mon. Wea. Rev.*, **130**, 610–628.
- , —, X. Gao, and S. Sorooshian, 2003: Short-term performance of MM5 with cloud-cover assimilation from satellite observations. *Mon. Wea. Rev.*, **131**, 1797–1810.

Copyright of *Monthly Weather Review* is the property of American Meteorological Society and its content may not be copied or emailed to multiple sites or posted to a listserv without the copyright holder's express written permission. However, users may print, download, or email articles for individual use.